Title
Enabling D2D Communications Through Neighbor Discovery in LTE Cellular Networks

Journal
IEEE Transactions on Signal Processing, 62(19)

ISSN
1053-587X

Authors
Tang, Huan
Ding, Zhi
Levy, Bernard C

Publication Date
2014

DOI
10.1109/tsp.2014.2348950

Peer reviewed

Enabling D2D Communications Through Neighbor Discovery in LTE Cellular Networks

Huan Tang, *Student Member, IEEE*, Zhi Ding, *Fellow, IEEE*, and Bernard C. Levy, *Fellow, IEEE*

***Abstract*—This work studies the problem of neighbor discovery for device-to-device (D2D) communications of LTE user equipments (UEs) in a modern cellular network. By listening to cellular uplink transmissions, UEs can detect potential D2D partners through a neighbor discovery process compatible with the standard LTE network protocol. We focus on neighbor discovery utilizing sounding reference signal (SRS) channel, which can be accessed by peer UEs that are LTE-compliant. Under the constraint of unknown channel statistics during uplink hearing, we propose joint neighbor detection and D2D channel estimation for listening UEs using the framework of sparse channel recovery. Composite hypothesis testing methods are further developed to refine neighbor detection accuracy. We evaluate the performance of our neighbor discovery methods under various network parameters to facilitate practical design and implementation of D2D in 4G cellular networks.**

***Index Terms*—Device-to-device communication, LTE uplink, detection, channel estimation.**

I. Introduction

THE rapid growth of mobile wireless data service continues to spur the expansion of high-rate and bandwidth-efficient wireless network systems. High volume data traffics in modern wireless system can lead to network overload, congestion, and process delay, severely straining the limited resource and capability of cellular networks. As a result, new connection modes such as device-to-device (D2D) has emerged as potential means to alleviate burden on radio network controllers (RNC) and eNodeBs (eNBs) [1]–[6].

In D2D enabled networks, direct radio links are allowed between cellular users for data transportation. One of the first steps in setting up D2D links involves pairing UEs that are in close proximity. This is accomplished during neighbor discovery process, where UEs will identify their neighbors for potential direct-link setup. In the multiuser context, neighbor discovery has been extensively studied [7]–[10]. In [7], multiuser detection based on a maximum likelihood approach is used for neighbor discovery. Considering the fact that the number of active users is relatively small compared with the total number of users, compressive sensing (CS) techniques have been recently introduced in [8]–[10], where user detection reduces to the classic problem of sparse vector recovery.

To facilitate the deployment of D2D functionality to standard LTE cellular systems, it is necessary to explore neighbor discovery opportunities in existing LTE infrastructure. Among current works on neighbor discovery in D2D scenario [3]–[6], few exploited practical LTE cellular systems. [3] elaborated a device beaconing scheme that forms a nerve system in the background of cellular traffics. A routing protocol for bidirectional communication was proposed in [5]. The authors of [6] considered neighbor discovery problem in LTE where the allocated OFDMA physical resource blocks are used as user identities. However, it is still not fully compatible with existing LTE systems in terms of scheduling and transmission signal sequence.

While additional resources are required to implement D2D neighbor discovery in [3]–[6], we develop new D2D neighbor discovery methods where the discovering UE identifies potential D2D partners by listening to cellular uplink channels. In particular, we utilize the SRS channel as a D2D neighbor discovery opportunity since it is a common uplink channel with potential transmissions from a large number of UEs, among which the discovering (listening) UE can identify transmitters in its proximity as candidates for D2D communication. Based on SRS channel structure, we formulate the problem of neighbor discovery using sparse channel recovery as a unified framework to implement joint neighbor detection and D2D channel estimation. We employ block sparse Bayesian learning (BSBL) for maximum likelihood estimation of D2D channel parameters. To improve neighbor detection performance, invariant tests based on composite hypothesis testing are investigated for designing detectors under a false alarm rate constraint. They are further combined with BSBL to recover D2D channel statistics.

We organize our manuscript as follows. Section II presents the basic system architecture within which we investigate effective methods for D2D neighbor discovery. Section III depicts the channel structure of SRS, which we exploit to formulate neighbor discovery as a sparse channel recovery problem. From Sections IV to VI, we focus on the discussion of various methods for neighbor detection. Neighbor discovery for devices with multiple antennas is studied in Section VII. Section VIII presents numerical results for performance evaluation before the conclusion section.

II. System Architecture

We consider a LTE cellular network that admits direct user communications. Authenticated UEs in the network have access

Manuscript received January 24, 2014; revised June 06, 2014; accepted August 02, 2014. Date of publication August 18, 2014; date of current version August 27, 2014. The associate editor coordinating the review of this manuscript and approving it for publication was Prof. Stefano Marano. This work was supported by the National Science Foundation under Grants CNS1147930, ECCS1307820, and CIF1321143.

The authors are with the Department of Electrical and Computer Engineering, University of California, Davis, CA 95616 USA (e-mail: hhtang@ucdavis.edu; zding@ucdavis.edu; bclevy@ucdavis.edu).

Color versions of one or more of the figures in this paper are available online at http://ieeexplore.ieee.org.

Digital Object Identifier 10.1109/TSP.2014.2348950

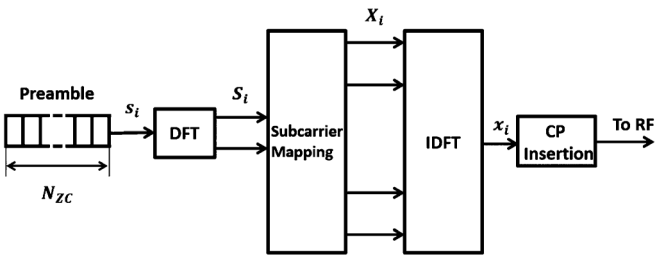

Fig. 1. Block diagram of SC-FDMA transmission at UE.

to the cellular base stations (eNBs) for regular cellular communications. At the same time, UEs can establish direct pairwise (D2D) links if permitted by the network. To set up D2D communication links, the initiating UE, denoted as UE-0, should learn about its neighbors in advance by listening to neighborhood UEs transmissions. In the cellular network, such UE transmission can be potentially captured during uplink periods. In a scheduled uplink time slot, if UE-0 is not transmitting to the eNB, it can listen to other UEs' uplink transmissions and thus identify UEs with high received SNR as neighbors. UE-0 can initiate D2D communication with neighbor UEs when it needs to transfer data to them. In the following, we will study neighbor discovery and D2D channel estimation methods based on cellular uplink hearing.

Throughout this paper, our discussion focuses on 3GPP LTE and LTE-A network signaling [11], [12]. We will first introduce basic time, frequency and multiplexing structure of LTE uplink. Based on this, UE transmissions in different uplink channels are compared regarding feasibility of implementing neighbor discovery. We identity SRS and PRACH as potential neighbor discovery opportunities since they are common uplink channels with potential transmissions from a large number of UEs in the network and it is possible for UE-0 to distinguish different UE transmissions with available information.

A. Basic Structure for LTE Uplink

1) Physical Resource Block (PRB): In LTE, the radio resources are allocated in unit of time-frequency physical resource block (PRB). Each PRB is comprised of 1 time slot in the time domain and 12 subcarriers in the frequency domain. Each time slot further consists of seven OFDM symbols.

2) Multiple Access Scheme: In LTE, multi-user access during uplink is enabled through SC-FDMA. As shown in Fig. 1, both DFT and IDFT are implemented at the transmitter in a SC-FDMA system to reduce peak-to-average-ratio (PAPR). For each OFDM symbol time, the time domain sequence is first transformed into frequency domain by the DFT block, before being mapped to a set of subcarriers. Different UEs are mapped to distinct sets of subcarriers, which enables the eNB to separate different UE signals in the frequency domain. After subcarrier mapping, the zero-filled frequency domain sequence is transformed back to the time domain. To mitigate inter-symbol interference, cyclic prefix is added to the time domain sequence before transmission.

TABLE I
UPLINK PHYSICAL CHANNELS

Channels	Function
PUSCH	Uplink data transmission
PUCCH	Uplink control signal transmission
PRACH	UE random access or reconnection
DM-RS	Channel estimation for coherent demodulation
SRS	Channel sounding for uplink scheduling

B. Physical Channels for LTE Uplink

The LTE uplink transmissions comprise of three physical channels and two reference signals as listed in Table I. We provide brief description of their relevance to neighbor discovery. To assess opportunities among these channels where UE-0 can discover its neighbors by eavesdropping on their uplink transmissions, we find it important for UE-0 to have some necessary information on potential transmitters in order to identify different UE transmissions. Since UE-0 does not have knowledge on UE uplink resource allocation, it is difficult to implement neighbor discovery based on signals carried by UE-specific channels. Therefore, we propose to use uplink channels shared by all UEs, such as PRACH and SRS, as potential opportunities for practical D2D neighbor discovery.

1) Dedicated Channels: The physical uplink shared channel (PUSCH) and the physical uplink control channel (PUCCH) are two dedicated channels used for uplink data transportation and control signaling, respectively. The eNB assigns different resources to different UEs such that their signal can be separated easily during uplink reception. Since both channels are modulated by UE-specific information, it is difficult for UE-0 to estimate the channel from its neighbors without knowing the specific transmitted data.

2) Reference Signals: There are two reference signals in LTE uplink. One is the demodulation reference signal (DM-RS) located in the middle of PUSCH. As a result, the frequency resources for DM-RS are UE-specific. Unless UE-0 knows fully the resource allocation of other UEs, neighbor discovery based on DM-RS would not be practical. On the other hand, the sounding reference signal (SRS) resides in the last OFDM symbol of each scheduled subframe. Since SRS is used for channel quality estimation to enable frequency-selective scheduling on the uplink, it is transmitted over a large bandwidth to obtain channel information across available subcarriers. Moreover, the subframes used for SRS is broadcasted within the network and known to all UEs. Hence, SRS provides a practical opportunity for neighbor discovery. The detailed discussion of D2D neighbor discovery in SRS is given later.

3) Random Access Channel: The physical random access (PRACH) allows UEs to initiate connection with the eNB during its cell entry stage or for reconnection. The PRBs for PRACH are semi-statistically allocated within the PUSCH region and are repeated periodically. During each PRACH time slot, a transmitting UE may randomly select a preamble from a predefined set to allow eNB to distinguish different UE transmissions. Since the preamble set is known to all UEs within the network, UE-0 is able to detect different preamble sequences as part of the neighbor discovery process. Given this feature, we identity PRACH as another potential neighbor

discovery opportunity. Due to different channel structure, the neighbor discovery methods in SRS cannot be directly applied to PRACH. However, they can be formulated in the common framework of sparse channel recovery. The solutions for PRACH neighbor discovery and D2D channel estimation will be discussed in a separate work.

III. Framework for Neighbor Discovery in LTE

In this section, we present problem formulation of neighbor discovery where a UE listens to neighborhood transmissions during the scheduled SRS symbol. We note that when a neighboring UE does not transmit in the corresponding SRS symbol, the listening UE cannot detect it. However, in practical LTE system, each UE is scheduled on the SRS channel regularly in order for the eNB to collect information for uplink channel scheduling. The listening UE can perform neighbor discovery across multiple SRS symbols to discover more neighbors. Moreover, the eNB can also help awaken a sleeping UE to transmit regularly on the SRS channel through paging channel to facilitate D2D discovery. In the following, we will focus on neighbor discovery within one SRS symbol. Without loss of generality, we denote the listening UE as UE-0 throughout this paper and assume that UE-0 listens to SRS channel only when it does not transmit in the corresponding SRS symbol. The proposed framework can be extended to PRACH.

A. Resource Allocation & Multiplexing

SRS is transmitted on the last SC-FDMA symbol in a subframe. The subframe is claimed by cell-specific broadcast signaling. Data transmission is blocked out in the SRS symbol. UEs are scheduled to transmit in SRS by the eNB and they are multiplexed via either frequency division multiplexing (FDM) or CDM. The system bandwidth is divided into disjoint sets of subcarriers. For each subcarrier set (SRS comb [20]), cyclic-shifted Zadoff-Chu (ZC) sequences are used for CDM by up to 8 UEs. The ZC sequence is expressed by

$$s_u(n) = \frac{1}{\sqrt{N}} \exp\left(-j2\pi u \frac{n(n+1)/2}{N}\right), \quad n = 0, \ldots, N-1.$$

u is called the root of the sequence and the sequence length N is an odd number. A ZC sequence has zero correlation with its cyclic-shifted copies and the absolute value of the correlation of two different-root ZC sequences is $\frac{1}{\sqrt{N}}$. Due to this nice property, ZC sequence is commonly adopted in LTE for CDM.

From the multiplexing structure in SRS, if UE-0 wants to distinguish different UEs' transmissions during SRS, it needs to know the allocation of SRS combs and the ZC sequences used for CDM on each SRS comb. In practice, the eNB can pass such information to UE-0 through downlink shared channel upon receiving a request for neighbor discovery.

B. SC-FDMA Transmitter and Receiver

Next we will discuss ZC sequence transmission and reception during SRS. Let $\boldsymbol{s}_i \in \mathcal{C}^{n_i}$ denote the ZC sequence used by UE-i. n_i is the sequence length. The discrete fourier transform (DFT) of $\boldsymbol{s}_i$ is expressed by $\boldsymbol{S}_i = \boldsymbol{F}_{n_i}\boldsymbol{s}_i$, where $\boldsymbol{F}_{n_i}$ denote the DFT matrix of size $n_i \times n_i$. Denote the SRS subcarrier mapping of UE-i based on Interleaved FDMA [20] by $\boldsymbol{\Gamma}_i$ of size $N \times n_i$, then $\boldsymbol{X}_i = \boldsymbol{\Gamma}_i \boldsymbol{S}_i$. N is the total number of subcarriers used for the IDFT $\boldsymbol{x}_i = \boldsymbol{F}_N^T \boldsymbol{X}_i$. Since zero-padding $\boldsymbol{X}_i$ results in an increased sampling rate in the time domain, $\boldsymbol{x}_i$ is an interpolated version of $\boldsymbol{s}_i$.

Before transmission, cyclic prefix (CP) is prepended to $\boldsymbol{x}_i$. We assume that the length of CP, denoted as L_{CP}, is larger than the sum of the maximum delay spread L_x and maximum round trip delay (RTD) $\delta_{\max,x}$ in the cell. After adding CP, the transmitted OFDM symbol is $[x_i(N-L_{\mathrm{CP}}), \ldots, x_i(N-1), x_i(0), \ldots, x_i(N-1)]$. The corresponding signal component $\boldsymbol{y}_i \in \mathcal{C}^{(N+L_{\mathrm{CP}})}$ received at UE-0 can be represented by the equation shown at the bottom of the page, where we used $[x_i'(0), \ldots, x_i'(N-1)]$ to denote the OFDM symbol transmitted before SRS.

Let N_{SC} denote the total number of SRS combs, then there are at most $U = 8N_{\mathrm{SC}}$ SRS transmitters. Due to that some $\boldsymbol{s}_i's$ may not be actively transmitted for a certain SRS opportunity, the actual number of transmitters may be smaller than U. By setting $\boldsymbol{h}_i = \boldsymbol{0}$ for those inactive ZC sequences, the received signal at UE-0 can be expressed in the following unified form

$$\boldsymbol{y}_{\mathrm{CP}} = \sum_{i=1}^{U} \boldsymbol{y}_{\mathrm{CP},i}(\delta_{i,x}) + \boldsymbol{z}_{\mathrm{CP}}, \tag{1}$$

where $\boldsymbol{y}_{\mathrm{CP},i}(\delta_{i,x})$ denotes the delayed version of $\boldsymbol{y}_{\mathrm{CP},i}$ by $\delta_{i,x}$ and $\boldsymbol{z}_{\mathrm{CP}}$ is the additive white Gaussian noise (AWGN). $\delta_{i,x}$ denotes the propagation delay from UE-i to UE-0.

From Fig. 2, the observation window at UE-0 is of length N and starts at position $L_{\mathrm{CP}} - \frac{\delta_{\max,x}}{2}$ of the SRS symbol. (Due to timing advance in LTE system, the earliest possible SRS transmission happens $\frac{\delta_{\max,x}}{2}$ before the SRS symbol.) Then the observed sequence at UE-0 is $\boldsymbol{y} = \sum_{i=1}^{U} \boldsymbol{y}_i + \boldsymbol{z}$ with (2), shown

$$\boldsymbol{y}_{\mathrm{CP},i} = \begin{bmatrix} x_i(N-L_{\mathrm{CP}}) & x_i'(N-1) & \cdots & x_i'(N-L_x+1) \\ x_i(N-L_{\mathrm{CP}}+1) & x_i(N-L_{\mathrm{CP}}) & \cdots & x_i'(N-L_x+2) \\ \vdots & & & \vdots \\ x_i(0) & x_i(N-1) & \cdots & x_i(N-L_x+1) \\ \vdots & & & \vdots \\ x_i(N-2) & x_i(N-3) & \cdots & x_i(N-L_x-1) \\ x_i(N-1) & x_i(N-2) & \cdots & x_i(N-L_x) \end{bmatrix} \underbrace{\begin{bmatrix} h_i(0) \\ h_i(1) \\ \vdots \\ h_i(L_x-1) \end{bmatrix}}_{\boldsymbol{h}_i}$$

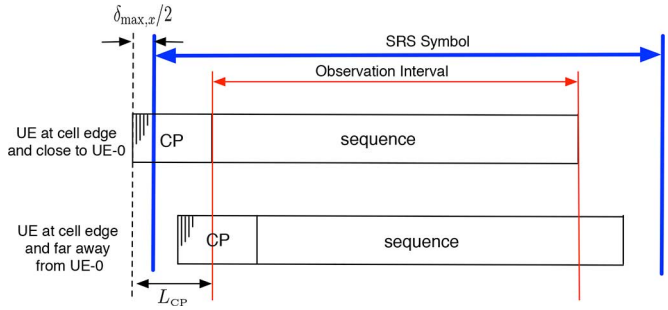

Fig. 2. Arrival of ZC sequences at UE-0.

at the bottom of the page, where $(\cdot)_N$ denotes the modulo-N operation. To separate signals from different SRS combs, UE-0 can demap the received signal in the frequency domain based on SRS comb information acquired from the eNB. Let $\boldsymbol{Y}, \boldsymbol{H}_i$ be the DFT of $\boldsymbol{y}, \boldsymbol{h}_i$, respectively, and denote $\boldsymbol{W}_1$ as the demapped SRS signal from the SRS comb used by UE-1, then $\boldsymbol{W}_1 = \boldsymbol{\Gamma}_1^T \boldsymbol{Y}$. Indexing the ZC sequences multiplexed on the first comb by 1 to 8, the kth element of $\boldsymbol{W}_1 \in \mathcal{C}^{n_i}$ is expressed by

$$\boldsymbol{W}_1(k) = \sum_{i=1}^{8} \boldsymbol{S}_i(k)\boldsymbol{H}_i(k) + \boldsymbol{Z}_1(k). \tag{3}$$

In standard LTE systems, the SRS receiver is designed for the eNB. The correlation of the received signal with different cyclic shifts of the root sequence can be used as channel impulse response (CIR) estimates of UEs on the same SRS comb [20]. The frequency domain channel estimates $\hat{\boldsymbol{H}}_i$ are then obtained by applying n_i-point DFT on the CIR estimates. While the eNB is able to maintain high SNR through uplink power control, UE-0 will possibly suffer from low receive SNR due to low transmission power or high propagation loss. Moreover, UE-0 does not know which ZC sequences are actively being transmitted. Therefore, active ZC sequence detection becomes a necessary step. Due to the uplink overhearing nature of D2D neighbor discovery, its SRS receiver design faces more challenges. We address the above problems by applying Bayesian learning and composite hypothesis testing, which can be used for signal detection and estimation with unknown parameters.

C. System Model

Before delving into the details of SRS receiver design, we will first present the system model for SRS. In order to take advantage of the correlation property of ZC sequences, transforming (3) to the time domain, we get $\boldsymbol{w}_1 = \sum_{i=1}^{8} \boldsymbol{r}_i + \boldsymbol{z}_1$ where, see (4) at the bottom of the page, $\boldsymbol{r}_i$ takes similar form as $\boldsymbol{y}_i$ in (2). Note that $\boldsymbol{x}_i$ and $\tilde{\boldsymbol{h}}_i$ are interpolated versions of $\boldsymbol{s}_i$ and $\boldsymbol{h}_i$, respectively. Therefore, $\delta_i = \lceil \frac{n_i}{N}\delta_{i,x} \rceil$, $L = \lceil \frac{n_i}{N} L_x \rceil$. To overcome the unknown delay of $\boldsymbol{s}_i$ in (4), we consider all possible cases for $\delta_i = 0, \ldots, \delta_{\max}$, where $\delta_{\max} = \lceil \frac{n_i}{N}\delta_{\max,x} \rceil$. Specifically, let $G = \delta_{\max} + L$, $\boldsymbol{r}_i$ can be written as

$$\boldsymbol{r}_i = \underbrace{\begin{bmatrix} s_i(0) & s_i(n_i-1) & \cdots & s_i(n_i-G+1) \\ s_i(1) & s_i(0) & \cdots & s_i(n_i-G+2) \\ \vdots & & & \vdots \\ s_i(n_i-1) & s_i(n_i-2) & \cdots & s_i(n_i-G) \end{bmatrix}}_{\boldsymbol{\Phi}_i} \times \underbrace{\begin{bmatrix} \mathbf{0} \\ \tilde{\boldsymbol{h}}_i \\ \mathbf{0} \end{bmatrix}}_{\boldsymbol{g}_i}. \tag{5}$$

$\tilde{\boldsymbol{h}}_i$ starts at the (δ_i+1)-th position in $\boldsymbol{g}_i$.

Based on (5), we get $\boldsymbol{w}_1 = \sum_{i=1}^{8} \boldsymbol{\Phi}_i \boldsymbol{g}_i + \boldsymbol{z}_1$. Applying the same transformation across N_{SC} SRS combs, the jointly received signal $\boldsymbol{w} := [\boldsymbol{w}_1^T, \ldots, \boldsymbol{w}_{N_{\mathrm{SC}}}^T]^T$ can be expressed by

$$\boldsymbol{w} = \underbrace{\begin{bmatrix} \boldsymbol{\Phi}_1 & \cdots & \boldsymbol{\Phi}_8 & \mathbf{0} & \cdots & \mathbf{0} \\ \mathbf{0} & & \ddots & & & \mathbf{0} \\ \mathbf{0} & & & \ddots & & \mathbf{0} \\ \mathbf{0} & \cdots & \mathbf{0} & \boldsymbol{\Phi}_{U-7} & \cdots & \boldsymbol{\Phi}_U \end{bmatrix}}_{\boldsymbol{\Psi}} \underbrace{\begin{bmatrix} \boldsymbol{g}_1 \\ \vdots \\ \vdots \\ \boldsymbol{g}_U \end{bmatrix}}_{\boldsymbol{g}} + \underbrace{\begin{bmatrix} \boldsymbol{z}_1 \\ \vdots \\ \vdots \\ \boldsymbol{z}_U \end{bmatrix}}_{\boldsymbol{z}}. \tag{6}$$

$\boldsymbol{\Psi} \in \mathcal{C}^{M_r \times M_c}$ with $M_r = \frac{1}{8}\sum_{i=1}^{U} n_i$ and $M_c = UG$. Due to that the columns of $\boldsymbol{\Phi}_i's$ on the same row are ZC sequences generated from the same root, $\boldsymbol{\Psi}^H\boldsymbol{\Psi} = \boldsymbol{I}_{M_c}$. Since each root sequence provides CDM for eight users, it is assumed that $n_i > 8G$ for all i. Consequently, $\boldsymbol{\Psi}$ is a tall matrix with full column

$$\boldsymbol{y}_i = \begin{bmatrix} x_i(N-\delta_{i,x})_N & x_i(N-\delta_{i,x}-1) & \cdots & x_i(N-\delta_{i,x}-L_x+1) \\ x_i(N-\delta_{i,x}+1)_N & x_i(N-\delta_{i,x}) & \cdots & x_i(N-\delta_{i,x}-L_x+2) \\ \vdots & & & \vdots \\ x_i(N-\delta_{i,x}-1) & x_i(N-\delta_{i,x}-2) & \cdots & x_i(N-\delta_{i,x}-L_x) \end{bmatrix} \underbrace{\begin{bmatrix} h_i(0) \\ \vdots \\ h_i(L_x-1) \end{bmatrix}}_{\boldsymbol{h}_i}, \tag{2}$$

$$\boldsymbol{r}_i = \begin{bmatrix} s_i(n_i-\delta_i)_{n_i} & s_i(n_i-\delta_i-1) & \cdots & s_i(n_i-\delta_i-L+1) \\ s_i(n_i-\delta_i+1)_{n_i} & s_i(n_i-\delta_i) & \cdots & s_i(n_i-\delta_i-L+2) \\ \vdots & & & \vdots \\ s_i(n_i-\delta_i-1) & s_i(n_i-\delta_i-2) & \cdots & s_i(n_i-\delta_i-L) \end{bmatrix} \underbrace{\begin{bmatrix} \tilde{h}_i(0) \\ \vdots \\ \tilde{h}_i(L-1) \end{bmatrix}}_{\tilde{\boldsymbol{h}}_i}. \tag{4}$$

rank. Denote the columns of $\boldsymbol{\Psi}$ containing $\boldsymbol{\Phi}_i$ as $\boldsymbol{\Psi}_i$, we can represent $\boldsymbol{w}$ by $\boldsymbol{w} = \sum_{i=1}^{U} \boldsymbol{\Psi}_i \boldsymbol{g}_i + \boldsymbol{z} = \boldsymbol{\Psi}\boldsymbol{g} + \boldsymbol{z}$.

D. Sparse Vector Recovery

Based on the system model in (6), our main purpose is to extract the stacked channel vector $\boldsymbol{g}$ from the noisy observation $\boldsymbol{w}$, given the knowledge of the coefficient matrix $\boldsymbol{\Psi}$. $\boldsymbol{g}$ is a block-sparse vector [13] that admits block structure corresponding to each UE. In this paper, we focus on the statistical model, assuming that the channel vectors and the noise vector follow independent complex Gaussian distribution. Specifically, $\boldsymbol{z} \sim \mathcal{CN}(0, \lambda \boldsymbol{I}_{M_r})$ where λ is the noise variance, $\boldsymbol{g}_i \sim \mathcal{CN}(0, \Sigma_{\boldsymbol{g}_i})$ where $\Sigma_{\boldsymbol{g}_i}$ has the structure

$$\Sigma_{\boldsymbol{g}_i} = \begin{bmatrix} \boldsymbol{0} & & \\ & \gamma_i \boldsymbol{I}_{L_i} & \\ & & \boldsymbol{0} \end{bmatrix}_{G \times G}. \tag{7}$$

γ_i and L_i are the channel variance and delay spread of UE-i, respectively. $\gamma_i = 0$ for the ZC sequences that are inactive. The nonzero diagonal entries in $\Sigma_{\boldsymbol{g}_i}$ starts at the $(\delta_i + 1)$-th position corresponding to the position of $\tilde{\boldsymbol{h}}_i$ in $\boldsymbol{g}_i$. From (6), $\boldsymbol{g} \sim \mathcal{CN}(0, \Sigma_{\boldsymbol{g}})$ with $\Sigma_{\boldsymbol{g}} = \mathrm{diag}(\Sigma_{\boldsymbol{g}_1}, \Sigma_{\boldsymbol{g}_2}, \ldots, \Sigma_{\boldsymbol{g}_U})$.

Using the statistical model above, recovering $\boldsymbol{g}$ can be interpreted as a pure estimation problem of the parameter set $\boldsymbol{\theta} = \{\{\gamma_i, \delta_i, L_i\}_{i=1}^{U}, \lambda\}$. By adopting the framework of block sparse bayesian learning (BSBL), $\boldsymbol{g}$ can be recovered using maximum a posteriori (MAP) criterion based on maximum likelihood (ML) estimate of $\boldsymbol{\theta}$. $\hat{\gamma}_i = 0$ indicates the corresponding $\boldsymbol{s}_i$ is not active. The problem can also be solved using two steps where detection is performed first to identify the nonzero blocks in $\boldsymbol{g}$ before employing ML estimation to find the parameters of the nonzero $\boldsymbol{g}_i's$.

Since UE-0 usually does not have the information of $\boldsymbol{\theta}$, it is difficult for it to detect nonzero $\boldsymbol{g}_i$ without any statistical information of the channel. In Chapter 11 of [16], detection of Gaussian signals with unknown parameters is formulated using the ML criterion, which extends to the BSBL method we present in Section IV. For pure detection with unknown signal parameters, uniform most powerful invariant (UMPI) and generalized likelihood ratio test (GLRT) are introduced in Chapter 5 of [16]. While UMPI tests only exist for certain classes of detection problems, GLRT is a more general method that is widely used. Our problem falls closest to case (iii) in Example 5.7 of [16], where a UMPI test for signal detection with unknown signal amplitude and unknown noise variance is devised. However, the unknown propagation delay δ_i and unknown delay spread L_i increase the difficulty in designing a UMPI test for the D2D neighbor discovery problem. To the best of the authors' knowledge, UMPI tests for similar problems have not been studied in the literature. We will describe more details of applying UMPI and GLRT to D2D neighbor discovery in Sections V and VI.

IV. Block Sparse Bayesian Learning (BSBL)

In this section, we will focus on using block sparse bayesian learning (BSBL) proposed in [13], [14] for sparse vector recovery given the system model (6). While uniform covariance structure is assumed in [13], [14] for each block, we are faced with the uncertainty of δ_i and L_i of each UE. However, by taking advantage of the orthogonality of $\boldsymbol{\Psi}_i$, $\boldsymbol{\theta}$ can be estimated using ML estimation in the BSBL framework.

A. Problem Formulation

In (6), given the statistical model of $\boldsymbol{g}$ and $\boldsymbol{z}$, the distribution of $\boldsymbol{w}$ is $\boldsymbol{w} \sim \mathcal{CN}(0, \Sigma_{\boldsymbol{w}})$ with $\Sigma_{\boldsymbol{w}} = \boldsymbol{\Psi}\Sigma_{\boldsymbol{g}}\boldsymbol{\Psi}^H + \lambda \boldsymbol{I}_{M_r}$. With the observed vector $\boldsymbol{w}$, the posterior density of $\boldsymbol{g}$ also follows Gaussian distribution denoted by $p(\boldsymbol{g} \,|\, \boldsymbol{w}, \Sigma_{\boldsymbol{g}}) \sim \mathcal{CN}(\boldsymbol{u}_{\mathrm{MAP}}, \Sigma_{\mathrm{MAP}})$ with

$$\boldsymbol{u}_{\mathrm{MAP}} = \Sigma_{\boldsymbol{g}}\boldsymbol{\Psi}^H \left(\boldsymbol{\Psi}\Sigma_{\boldsymbol{g}}\boldsymbol{\Psi}^H + \lambda \boldsymbol{I}_{M_r}\right)^{-1} \boldsymbol{w}, \tag{8a}$$

$$\Sigma_{\mathrm{MAP}} = \Sigma_{\boldsymbol{g}} - \Sigma_{\boldsymbol{g}}\boldsymbol{\Psi}^H \left(\boldsymbol{\Psi}\Sigma_{\boldsymbol{g}}\boldsymbol{\Psi}^H + \lambda \boldsymbol{I}_{M_r}\right)^{-1} \boldsymbol{\Psi}\Sigma_{\boldsymbol{g}}. \tag{8b}$$

The essential idea of Bayesian learning is that the observation $\boldsymbol{w}$ can provide additional evidence to refine the estimate of $\boldsymbol{g}$, which is performed by maximizing $p(\boldsymbol{g} \,|\, \boldsymbol{w}, \Sigma_{\boldsymbol{g}})$. For known $\boldsymbol{\theta}$, the maximum a posterior (MAP) estimate of $\boldsymbol{g}$ can be derived directly as

$$\hat{\boldsymbol{g}} = \boldsymbol{u}_{\mathrm{MAP}}. \tag{9}$$

For $\boldsymbol{u}_{\mathrm{MAP}}$ with unknown paramters, the critical issue of Bayesian learning lies in parameter estimation. Using ML criterion, the parameter estimation in BSBL is expressed by

$$\underset{\boldsymbol{\theta}}{\text{Maximize}} \quad \log p(\boldsymbol{w} \mid \boldsymbol{\theta})$$

which, after substituting the distribution of $\boldsymbol{w}$, is equivalent to

$$\underset{\boldsymbol{\theta}}{\text{Minimize}} \quad \xi_S = \log|\Sigma_{\boldsymbol{w}}| + \boldsymbol{w}^H \Sigma_{\boldsymbol{w}}^{-1} \boldsymbol{w}. \tag{10}$$

B. Maximum Likelihood Estimation

Next we discuss solving (10) for the neighbor discovery model in (6). Considering the block structure of $\Sigma_{\boldsymbol{g}}$ and that $\boldsymbol{\Psi}$ has orthonormal columns, we can decompose (10) with respect to each block. First, denote

$$\bar{\boldsymbol{\Psi}} = [\boldsymbol{\Psi}\, \boldsymbol{\Psi}_{U+1}],$$

where $\boldsymbol{\Psi}_{U+1}$ is the null space of $\boldsymbol{\Psi}^H$ with $K = M_r - M_c$ orthonormal columns. Correspondingly, $\Sigma_{\boldsymbol{g}}$ can be expanded into diagonal matrix $\bar{\Sigma}_{\boldsymbol{g}}$ by padding K zeros on the diagonal. Substitute $\bar{\boldsymbol{\Psi}}$ and $\bar{\Sigma}_{\boldsymbol{g}}$ into (10), we get

$$\xi_S = \log\left|\Sigma_{\boldsymbol{g}}\boldsymbol{\Psi}^H\boldsymbol{\Psi} + \lambda \boldsymbol{I}_{M_c}\right| + K\log\lambda + \boldsymbol{w}^H \bar{\boldsymbol{\Psi}} \left(\bar{\Sigma}_{\boldsymbol{g}} + \lambda \boldsymbol{I}_{M_r}\right)^{-1} \bar{\boldsymbol{\Psi}}^H \boldsymbol{w}. \tag{11}$$

Let $\boldsymbol{v}_i := \boldsymbol{\Psi}_i^H \boldsymbol{w} = \boldsymbol{g}_i + \boldsymbol{\Psi}_i^H \boldsymbol{z}$ for $i = 1, \ldots, U+1$, we can decompose (11) as

$$\xi_S = \sum_{i=1}^{U} \left[\log\left|\Sigma_{\boldsymbol{g}_i} + \lambda \boldsymbol{I}_G\right| + \boldsymbol{v}_i^H \left(\Sigma_{\boldsymbol{g}_i} + \lambda \boldsymbol{I}_G\right)^{-1} \boldsymbol{v}_i\right] + K\log\lambda + \frac{\|\boldsymbol{v}_{U+1}\|_2^2}{\lambda}. \tag{12}$$

The terms in the square bracket can be further transformed as

$$\xi_S^{(i)} := L_i \log(\lambda + \gamma_i) + (G - L_i)\log\lambda + \frac{\|\boldsymbol{v}_{i,L_i}\|_2^2}{\lambda + \gamma_i} + \frac{\left\|\boldsymbol{v}_{i,L_i^c}\right\|_2^2}{\lambda},$$

where $\boldsymbol{v}_{i,L_i}$ denotes the L_i consecutive elements within $\boldsymbol{v}_i$ starting at the (δ_i+1)-th position, whereas $\boldsymbol{v}_{i,L_i^c}$ denotes the remaining entries. Assign $\xi_S^{(U+1)} := K\log\lambda + \frac{\|\boldsymbol{v}_{U+1}\|_2^2}{\lambda}$. Then $\xi_S = \sum_{i=1}^{U+1}\xi_S^{(i)}$.

To minimize ξ_S, we first note that for $\gamma_i \geq 0$, $\xi_S^{(i)}$ is minimized when $\boldsymbol{v}_{i,L_i}$ is taken as the L_i consecutive elements in $\boldsymbol{v}_i$ with the largest l_2-norm (energy), which gives the estimate of δ_i. To estimate $\{\gamma_i\}_{i=1}^U$, we can start by extracting the terms related γ_i, which we denote as

$$f_{\gamma_i}(\gamma_i) = L_i\log(\gamma_i+\lambda) + \frac{\|\boldsymbol{v}_{i,L_i}\|_2^2}{\gamma_i+\lambda}.$$

For given L_i and λ, the minimizer of $f_{\gamma_i}(\gamma_i)$ is given by

$$\hat{\gamma}_i = \max\left(\frac{\|\boldsymbol{v}_{i,L_i}\|_2^2}{L_i} - \lambda, 0\right) =: \left(\frac{\|\boldsymbol{v}_{i,L_i}\|_2^2}{L_i} - \lambda\right)^+. \tag{13}$$

Correspondingly,

$$f_{\gamma_i}(\hat{\gamma}_i) = \begin{cases} L_i\log\lambda + \frac{\|\boldsymbol{v}_{i,L_i}\|_2^2}{\lambda}, & \lambda > \frac{\|\boldsymbol{v}_{i,L_i}\|_2^2}{L_i} \\ L_i\log\frac{\|\boldsymbol{v}_{i,L_i}\|_2^2}{L_i} + L_i, & \text{otherwise} \end{cases}. \tag{14}$$

Substituting $\hat{\gamma}_i$ into $\xi_S^{(i)}$, we get (15), shown at the bottom of the page. Since the second expression in (15) is no larger than the first expression, L_i is estimated as

$$\hat{L}_i = \underset{\substack{L_i\in\{1,\ldots,L\} \\ \|\boldsymbol{v}_{i,L_i}\|_2^2/L_i\geq\lambda}}{\arg\min} \left\{ L_i\log\frac{\|\boldsymbol{v}_{i,L_i}\|_2^2}{L_i\lambda} + L_i + \frac{\left\|\boldsymbol{v}_{i,L_i^c}\right\|_2^2}{\lambda} \right\}. \tag{16}$$

Note that $\max_{L_i}\frac{\|\boldsymbol{v}_{i,L_i}\|_2^2}{L_i} = \max_j|v_{i,j}|^2$, where $v_{i,j}$ is the j-th element of $\boldsymbol{v}_i$. From (15), when $\max_j|v_{i,j}|^2 < \lambda$, we can take $\hat{L}_i = 0$ and $\hat{\gamma}_i = 0$. Denote

$$\mathcal{I} = \left\{ i : \max_j |v_{ij}|^2 \geq \lambda \right\}. \tag{17}$$

Substituting (15) into (12), we have

$$\xi_S = \sum_{i\in\mathcal{I}}\left[\hat{L}_i\log\frac{\left\|\boldsymbol{v}_{i,\hat{L}_i}\right\|_2^2}{\hat{L}_i\lambda} + \hat{L}_i + G\log\lambda + \frac{\left\|\boldsymbol{v}_{i,\hat{L}_i^c}\right\|_2^2}{\lambda}\right] + \sum_{i\notin\mathcal{I}}\left[G\log\lambda + \frac{\|\boldsymbol{v}_i\|_2^2}{\lambda}\right] + K\log\lambda + \frac{\|\boldsymbol{v}_{U+1}\|_2^2}{\lambda},$$

whose minimizer is given by

$$\hat{\lambda} = \frac{\sum_{i=1}^{U+1}\|\boldsymbol{v}_i\|_2^2 - \sum_{i\in\mathcal{I}}\left\|\boldsymbol{v}_{i,\hat{L}_i}\right\|_2^2}{UG + K - \sum_{i\in\mathcal{I}}\hat{L}_i}. \tag{18}$$

Since $\hat{\lambda}$, $\mathcal{I}$ and $\hat{L}_i$ are mutually dependent, we update the estimates iteratively starting with $\hat{\lambda}^{(0)}$ and then applying (16), (17) and (18) alternatively until ξ_S no longer decreases. Since both (16) and (18) reduce ξ_S and ξ_S is lower bounded by

$$\check{\xi}_S = \sum_{i=1}^{U}\check{\xi}_S^{(i)} + K\log\frac{\|\boldsymbol{v}_{U+1}\|_2^2}{K} + K, \tag{19}$$

where $\check{\xi}_S^{(i)}$ is the lower bound of $\xi_S^{(i)}$ in (15) given by

$$\check{\xi}_S^{(i)} = \min_{L_i}\left\{ L_i\log\frac{\|\boldsymbol{v}_{i,L_i}\|_2^2}{L_i} + (G-L_i)\log\frac{\|\boldsymbol{v}_{i,L_i^c}\|_2^2}{G-L_i} + G \right\}, \tag{20}$$

the iteration will converge. The convergence point depends on $\hat{\lambda}^{(0)}$, which can be estimated from the noise subspace as

$$\hat{\lambda}^{(0)} = \frac{\|\boldsymbol{v}_{U+1}\|_2^2}{K}. \tag{21}$$

Note that $\boldsymbol{v}_i = \boldsymbol{\Psi}_i\boldsymbol{w}$ is the correlation of the received signal with different ZC sequences. Therefore, BSBL can be applied to the correlation-based SRS receiver designed for the eNB [20]. In the next two sections, we will discuss neighbor detection method where detection is considered first and parameter estimation is implemented based on the detection results. They can also be adopted by the eNB SRS receiver through $\boldsymbol{v}_i$.

V. Invariant Tests

In this section, we will discuss using the uniformly most power invariant (UMPI) framework to devise detector for active ZC sequences. An important feature of invariant tests is that the detection rule does not rely on the unknown parameters, which therefore enables detection without knowing certain parameters. Following the UMPI framework, we will start with the discussion of the transformation group that leaves the detection problem invariant. After establishing the maximum invariant statistic of the transformation group, we derive the likelihood ratio of the maximum invariant statistic. The likelihood ratio is approximated in the low SNR and high SNR, respectively, which give us detection rules that is independent of $\boldsymbol{\theta}$.

$$\xi_S^{(i)} = \begin{cases} G\log\lambda + \frac{\|\boldsymbol{v}_i\|_2^2}{\lambda}, & \lambda > \frac{\|\boldsymbol{v}_{i,L_i}\|_2^2}{L_i} \\ L_i\log\frac{\|\boldsymbol{v}_{i,L_i}\|_2^2}{L_i\lambda} + L_i + G\log\lambda + \frac{\|\boldsymbol{v}_{i,L_i^c}\|_2^2}{\lambda}, & \text{otherwise} \end{cases}. \tag{15}$$

A. Transformation Group

To detect the existence of UE-i, we focus on

$$\boldsymbol{p}_i = \begin{bmatrix} \boldsymbol{v}_i \\ \boldsymbol{v}_{U+1} \end{bmatrix} = \begin{bmatrix} \boldsymbol{\Psi}_i^H \boldsymbol{w} \\ \boldsymbol{\Psi}_{U+1}^H \boldsymbol{w} \end{bmatrix} = \begin{bmatrix} \boldsymbol{g}_i + \boldsymbol{\Psi}_i^H \boldsymbol{z} \\ \boldsymbol{\Psi}_{U+1}^H \boldsymbol{z} \end{bmatrix}$$

which corresponds to the i-th UE block and the noise block. From the distribution of $\boldsymbol{g}_i$ and $\boldsymbol{z}$, $\boldsymbol{p}_i \sim \mathcal{CN}(\boldsymbol{0}, \boldsymbol{\Sigma}_{\boldsymbol{p}_i})$ with

$$\boldsymbol{\Sigma}_{\boldsymbol{p}_i} = \begin{bmatrix} \boldsymbol{\Sigma}_{\boldsymbol{g}_i} + \lambda \boldsymbol{I}_G & \\ & \lambda \boldsymbol{I}_K \end{bmatrix},$$

where $\{\gamma, \delta_i, L_i\}$ embedded in $\boldsymbol{\Sigma}_{\boldsymbol{g}_i}$ and λ are all unknown. Let $\boldsymbol{\theta}_i = \{\gamma, \delta_i, L_i, \lambda\}$. The hypotheses can be expressed by

$$\mathcal{H}_0 : \boldsymbol{\theta}_i \in \boldsymbol{\Theta}_0, \qquad \boldsymbol{\Theta}_0 = \{\boldsymbol{\theta}_i : \gamma_i = 0\}, \tag{22a}$$

$$\mathcal{H}_1 : \boldsymbol{\theta}_i \in \boldsymbol{\Theta}_1, \qquad \boldsymbol{\Theta}_1 = \{\boldsymbol{\theta}_i : \gamma_i > 0\}. \tag{22b}$$

From [16], a detection problem is invariant under a transformation group if the distribution remains in the same family and the parameter spaces are preserved. To preserve the Gaussianity of $\boldsymbol{p}_i$, we only consider affine transformations given by $g(\boldsymbol{p}_i) = \boldsymbol{A}\boldsymbol{p}_i + \boldsymbol{b}$. Since $\boldsymbol{p}_i$ has zero mean under both hypotheses, $\boldsymbol{b} = \boldsymbol{0}$. Moreover, from the block diagonal structure of $\boldsymbol{\Sigma}_{\boldsymbol{p}_i}$, $\boldsymbol{A}$ also needs to be block diagonal. Denote

$$\boldsymbol{A} = \begin{bmatrix} \boldsymbol{A}_1 & \\ & \boldsymbol{A}_2 \end{bmatrix},$$

then

$$\boldsymbol{\Sigma}_{g(\boldsymbol{p}_i)} = \begin{bmatrix} \boldsymbol{A}_1 \boldsymbol{\Sigma}_{\boldsymbol{g}_i} \boldsymbol{A}_1^H + \lambda \boldsymbol{A}_1 \boldsymbol{A}_1^H & \\ & \lambda \boldsymbol{A}_2 \boldsymbol{A}_2^H \end{bmatrix}.$$

Due to the uncertainty of δ_i, we can consider the transformation group consisting of applying a cyclic shift [18] to $\boldsymbol{v}_i$. Specifically, let $\boldsymbol{P}_j$ be a permutation matrix such that $\boldsymbol{P}_j \boldsymbol{v}_i$ represents a cyclic shift of $\boldsymbol{v}_i$ by j places. Then $\boldsymbol{A}_1$ can be taken from $\mathcal{P} := \{\boldsymbol{P}_j, j = 1, \ldots, G\}$. The matrix $\boldsymbol{A}_2$ is selected as a unitary matrix satisfying $\boldsymbol{A}_2 \boldsymbol{A}_2^H = \boldsymbol{A}_2^H \boldsymbol{A}_2 = \boldsymbol{I}_K$.

Define $\mathcal{A} = \{\mathrm{diag}(\boldsymbol{A}_1, \boldsymbol{A}_2) : \boldsymbol{A}_1 \in \mathcal{P}, \boldsymbol{A}_2 \in \mathcal{U}_K\}$ where $\mathcal{U}_K$ is the set of unitary matrices of size K. The induced transformation on the parameter space under the transformation group

$$\mathcal{G} = \{g : g(\boldsymbol{p}_i) = c\boldsymbol{A}\boldsymbol{p}_i, c \in \mathbb{R}, c \neq 0, \boldsymbol{A} \in \mathcal{A}\} \tag{23}$$

is given by

$$\bar{g}(\boldsymbol{\theta}_i) = \bar{g}(\{\gamma, \delta_i, L_i, \lambda\}) = \{c^2\gamma_i, [\delta_i + j]_G, L_i, c^2\lambda\}$$

where $[\cdot]_G$ denotes the modulo-G operation. Since $c \neq 0$, $\bar{g}(\boldsymbol{\theta}_i) \in \Theta_0$ if and only if $\boldsymbol{\theta}_i \in \Theta_0$ and $\bar{g}(\boldsymbol{\theta}_i) \in \Theta_1$ if and only if $\boldsymbol{\theta}_i \in \Theta_1$. Therefore, (22) is invariant under $\mathcal{G}$.

B. Maximal Invariant Statistic

Next we will discuss the maximum invariant statistic of the transformation group (23). The definition of maximum invariant statistic is given below following [16]. A test is *invariant* if it can be expressed as a function of a maximal invariant statistic.

Definition 1 (Maximal Invariant Statistic): When $\boldsymbol{p}_i$ admits invariant distribution under the transformation group $\mathcal{G}$, $S(\boldsymbol{p}_i)$ is a *maximal invariant statistic* if

1) $S(g(\boldsymbol{p}_i)) = S(\boldsymbol{p}_i)$;

2) $S(\boldsymbol{p}_i') = S(\boldsymbol{p}_i)$ implies $\boldsymbol{p}_i' = g(\boldsymbol{p}_i)$ for some $g \in \mathcal{G}$. ■

Based on [18], a maximal invariant statistic under the transformation group in (23) is given in Theorem 1. The form of $S(\boldsymbol{p}_i)$ results naturally from the scale invariance of the detection problem (22). $\boldsymbol{P}_{j_*}$ aligns shifted versions of $\boldsymbol{v}_i$ to the same position. Hence it is a maximal invariant statistic to the shifts of $\boldsymbol{v}_i$. The method of selecting $\boldsymbol{P}_{j_*}$ is not unique, but all selection schemes will build an equivalence class containing $\boldsymbol{v}_i$ and its circular cyclic shifts.

Theorem 1: A *maximal invariant statistic* to the transformation group $\mathcal{G} = \{g : g(\boldsymbol{p}_i) = c\boldsymbol{A}\boldsymbol{p}_i, c \in \mathbb{R}, c \neq 0, \boldsymbol{A} \in \mathcal{A}\}$ is

$$S(\boldsymbol{p}_i) = \frac{\boldsymbol{P}_{j_*} \boldsymbol{v}_i}{\|\boldsymbol{v}_{U+1}\|_2} \tag{24}$$

where j_* is selected such that the first L elements of $\boldsymbol{P}_{j_*} \boldsymbol{v}_i$ has the maximum l_2-norm among all L circularly consecutive elements of $\boldsymbol{v}_i$.

Proof: See Appendix A. ■

C. Likelihood Ratio

Given a maximal invariant statistic, the UMPI test is built upon the likelihood ratio test (LRT) of $S(\boldsymbol{p}_i)$ under two hypotheses. We will start by investigating the statistic of $S(\boldsymbol{p}_i)$.

Note that $S(\boldsymbol{p}_i)$ is the ratio of two independent random variables, we can express its PDF by

$$f_{S(\boldsymbol{p}_i)}(\boldsymbol{x}) = \int_0^\infty \tau f_{\boldsymbol{P}_{j_*} \boldsymbol{v}_i}(\tau \boldsymbol{x}) f_{\|\boldsymbol{v}_{U+1}\|_2}(\tau) d\tau. \tag{25}$$

Since $\frac{1}{\sqrt{\lambda}} \|\boldsymbol{v}_{U+1}\|_2 \sim \chi(2K)$, we have

$$f_{\|\boldsymbol{v}_{U+1}\|_2}(x) = \frac{2^{1-K} \lambda^{-K}}{\Gamma(K)} x^{2K-1} \exp\left(-\frac{x^2}{2\lambda}\right).$$

Moreover, following a similar approach in [18], the PDF of $\boldsymbol{P}_{j_*} \boldsymbol{v}_i$ can be expressed by

$$\begin{aligned} f_{\boldsymbol{P}_{j_*} \boldsymbol{v}_i}(\boldsymbol{x}) &= \sum_{j=1}^{G} \frac{\exp\left(-\boldsymbol{x}^H \boldsymbol{P}_j^H \boldsymbol{\Sigma}_{\boldsymbol{v}_i}^{-1} \boldsymbol{P}_j \boldsymbol{x}\right)}{\pi^G |\boldsymbol{\Sigma}_{\boldsymbol{v}_i}|} \\ &= \frac{1}{\pi^G (\gamma_i + \lambda)^{L_i} \lambda^{G - L_i}} \\ &\quad \times \sum_{j=1}^{G} \exp\left[-\left(\frac{\|\boldsymbol{x}_{j,L_i}\|_2^2}{\gamma_i + \lambda} + \frac{\left\|\boldsymbol{x}_{j,L_i^c}\right\|_2^2}{\lambda}\right)\right], \end{aligned}$$

where $\boldsymbol{x}_{j,L_i}$ denotes L_i circularly consecutive elements in $\boldsymbol{x}$ starting at the j-th position and $\boldsymbol{x}_{j,L_i^c}$ is the complement elements of $\boldsymbol{x}_{j,L_i}$ in $\boldsymbol{x}$. Substituting $f_{\boldsymbol{P}_{j_*} \boldsymbol{v}_i}(\boldsymbol{x})$ into (25), we have

$$\begin{aligned} &f_{S(\boldsymbol{p}_i)}(\boldsymbol{x}) \\ &\quad = \sum_{j=1}^{G} \int_0^\infty \frac{c_1 \tau^{2K}}{\exp\left[\left(\frac{\|\boldsymbol{x}_{j,L_i}\|_2^2}{\gamma_i + \lambda} + \frac{\left\|\boldsymbol{x}_{j,L_i^c}\right\|_2^2}{\lambda} + \frac{1}{2\lambda}\right)\tau^2\right]} d\tau \end{aligned}$$

with $c_1 = \frac{2^{1-K} \lambda^{-K}}{\pi^G (\gamma_i + \lambda)^{L_i} \lambda^{G - L_i} \Gamma(K)}$. Since

$$\int_0^\infty \tau^{2K} \exp(-c\tau^2) d\tau = \frac{0.5}{c^{K+0.5}} \Gamma(K + 0.5),$$

we get

$$f_{S(\boldsymbol{p}_i)}(\boldsymbol{x}) = \sum_{j=1}^{G} \frac{0.5c_1\Gamma(K+0.5)}{\left(\frac{\|\boldsymbol{x}_{j,L_i}\|_2^2}{\gamma_i+\lambda} + \frac{\left\|\boldsymbol{x}_{j,L_i^c}\right\|_2^2}{\lambda} + \frac{1}{2\lambda}\right)^{(K+0.5)}}.$$

Hence, the LRT of $S(\boldsymbol{p}_i)$ is given by

$$\begin{aligned} &L(S(\boldsymbol{p}_i)) \\ &= \frac{f_{S(\boldsymbol{p}_i)}(S(\boldsymbol{p}_i) \mid \gamma_i \neq 0)}{f_{S(\boldsymbol{p}_i)}(S(\boldsymbol{p}_i) \mid \gamma_i = 0)} \\ &= \frac{\sum_{j=1}^{G}\left(\frac{\left\|S(\boldsymbol{p}_i)_{j,L_i}\right\|_2^2}{\gamma_i+\lambda} + \frac{\left\|S(\boldsymbol{p}_i)_{j,L_i^c}\right\|_2^2}{\lambda} + \frac{1}{2\lambda}\right)^{-(K+0.5)}}{G(1+\gamma_i/\lambda)^{L_i}\left(\frac{\|S(\boldsymbol{p}_i)\|_2^2}{\lambda} + \frac{1}{2\lambda}\right)^{-(K+0.5)}} \\ &= \frac{\sum_{j=1}^{G}\left[1 - \frac{\left(1-\frac{1}{\gamma_i/\lambda+1}\right)\left\|S(\boldsymbol{p}_i)_{j,L_i}\right\|_2^2}{\|S(\boldsymbol{p}_i)\|_2^2+0.5}\right]^{-(K+0.5)}}{G(1+\gamma_i/\lambda)^{L_i}}, \end{aligned}$$

for which the sufficient statistic is

$$T(\boldsymbol{p}_i) = \sum_{j=1}^{G}\left[1 - \frac{\left(1-\frac{1}{\gamma_i/\lambda+1}\right)\left\|S(\boldsymbol{p}_i)_{j,L_i}\right\|_2^2}{\|S(\boldsymbol{p}_i)\|_2^2+0.5}\right]^{-(K+0.5)}.$$

Since $T(\boldsymbol{p}_i)$ depends on the unknown quantities γ_i/λ and L_i, the LRT cannot be expressed as a uniform most powerful invariant (UMPI) test. Nevertheless, when the lowest order term of the sufficient statistic is a monotone function of a scalar statistic, the detector is a locally most powerful invariant (LMPI) test [19]. We will derive the LMPI detector in the low SNR case. For high SNR, we develop a constant false alarm rate (CFAR) detector based on the approximation of $T(\boldsymbol{p}_i)$.

D. Invariant Tests

1) Low SNR: For low SNR case with $\gamma_i/\lambda \ll 1$, $\frac{1}{\gamma_i/\lambda+1} \approx 1-\gamma_i/\lambda$. Therefore,

$$\frac{\left(1-\frac{1}{\gamma_i/\lambda+1}\right)\left\|S(\boldsymbol{p}_i)_{j,L_i}\right\|_2^2}{\|S(\boldsymbol{p}_i)\|_2^2+0.5} \approx \frac{\frac{\gamma_i}{\lambda}\left\|S(\boldsymbol{p}_i)_{j,L_i}\right\|_2^2}{\|S(\boldsymbol{p}_i)\|_2^2+0.5} \ll 1.$$

Using the result that $(1+x)^\alpha \approx 1+\alpha x$ for $|x| \ll 1$, $T(\boldsymbol{p}_i)$ can be approximated by

$$\begin{aligned} T(\boldsymbol{p}_i) &\approx \sum_{j=1}^{G}\left[1 + (K+0.5)\frac{\left(1-\frac{1}{\gamma_i/\lambda+1}\right)\left\|S(\boldsymbol{p}_i)_{j,L_i}\right\|_2^2}{\|S(\boldsymbol{p}_i)\|_2^2+0.5}\right] \\ &= G + L_i(K+0.5)\frac{\left(1-\frac{1}{\gamma_i/\lambda+1}\right)\|S(\boldsymbol{p}_i)\|_2^2}{\|S(\boldsymbol{p}_i)\|_2^2+0.5}. \end{aligned}$$

Since $1-\frac{1}{\gamma_i/\lambda+1} > 0$, $T(\boldsymbol{p}_i)$ is a monotonically increasing function of $\|S(\boldsymbol{p}_i)\|_2^2$. Hence, the LMPI test for low SNR can be expressed by

$$(\textbf{LMPI}) \quad \|S(\boldsymbol{p}_i)\|_2^2 = \frac{\|\boldsymbol{v}_i\|_2^2}{\|\boldsymbol{v}_{U+1}\|_2^2} \underset{H_0}{\overset{H_1}{\gtrless}} \eta. \tag{26}$$

The false alarm probability of (26) is expressed by

$$\begin{aligned} P_F &= \Pr\left(\|S(\boldsymbol{p}_i)\|_2^2 > \eta \mid \mathcal{H}_0\right) \\ &= \int_{\eta}^{\infty} f_{\|S(\boldsymbol{p}_i)\|_2^2}(x \mid \gamma_i = 0)dx. \end{aligned}$$

Since $\|\boldsymbol{v}_i\|_2^2/\lambda \sim \chi^2(2G)$ under hypothesis $\mathcal{H}_0$ and $\|\boldsymbol{v}_{U+1}\|_2^2/\lambda \sim \chi^2(2K)$, $\|S(\boldsymbol{p}_i)\|_2^2$ follows F distribution under hypothesis $\mathcal{H}_0$. Hence, P_F can be expressed using the CDF of the F distribution, which is given by

$$P_F = \frac{1}{(\eta+1)^{G+K-1}} \sum_{j=G}^{G+K-1}\binom{G+K-1}{j}\eta^j.$$

For a target false alarm rate α, η can be set accordingly.

2) High SNR: For large γ_i/λ, $1-\frac{1}{\gamma_i/\lambda+1} \approx 1$. As a result,

$$T(\boldsymbol{p}_i) \approx \sum_{j=1}^{G}\left(1 - \frac{\left\|S(\boldsymbol{p}_i)_{j,L_i}\right\|_2^2}{\|S(\boldsymbol{p}_i)\|_2^2+0.5}\right)^{-(K+0.5)},$$

which is independent of γ_i/λ but depends on L_i. However, since $T(\boldsymbol{p}_i)$ is monotonically increasing with L_i, we can consider the test

$$(\textbf{CFAR}) \quad \sum_{j=1}^{G}\left(1 - \frac{\left\|S(\boldsymbol{p}_i)_{j,1}\right\|_2^2}{\|S(\boldsymbol{p}_i)\|_2^2+0.5}\right)^{-(K+0.5)} \underset{H_0}{\overset{H_1}{\gtrless}} \eta \tag{27}$$

as the worst-case test. Note indeed that for a fixed η, the statistic $T(\boldsymbol{p}_i)$ with $L_i = 1$ is the one that yields the lowest probability of detection. Similar to (26), (27) does not depend on λ under hypothesis $\mathcal{H}_0$ and is hence a CFAR detector. There is no closed form of the false alarm probability in this case. Given a target value of P_F, the detection threshold η can be set numerically.

E. D2D Channel Estimation

Let $\mathcal{I}$ denote the index set of the active ZC sequences determined from the detection step. Next we will discuss parameter estimation for $i \in \mathcal{I}$ employing the BSBL framework discussed in Section IV. The MAP estimate of $\boldsymbol{g}_i$ is further derived based on the estimated parameters.

Given $\mathcal{I}$, the initial noise variance estimate can be obtained from the augmented noise subspace as

$$\hat{\lambda}^{(0)} = \frac{\sum_{i\notin\mathcal{I}}\|\boldsymbol{v}_i\|_2^2 + \|\boldsymbol{v}_{U+1}\|_2^2}{G(U-|\mathcal{I}|)+K}. \tag{28}$$

Then we can apply (16) and (18) to update $\hat{L}_i$ and $\hat{\lambda}$ alternatively until ξ_S converges. Further, $\hat{\gamma}_i = (\frac{\|\boldsymbol{v}_{i,\hat{L}_i}\|_2^2}{\hat{L}_i} - \hat{\lambda})^+$. $\hat{\delta}_i$ can be estimated from the position of $\boldsymbol{v}_{i,\hat{L}_i}$. Recall that $\hat{\boldsymbol{g}} = \boldsymbol{u}_{\mathrm{MAP}}$. Decomposing the expression of $\boldsymbol{u}_{\mathrm{MAP}}$ in (8a) into each UE block, we have

$$\hat{\boldsymbol{g}}_i = \hat{\Sigma}_{\boldsymbol{g}_i} \left(\hat{\Sigma}_{\boldsymbol{g}_i} + \lambda \boldsymbol{I}_G\right)^{-1} \boldsymbol{v}_i, \tag{29}$$

where $\hat{\Sigma}_{\boldsymbol{g}_i}$ takes the form in (7) and can be obtained from $\hat{\gamma}_i, \hat{\delta}_i$ and $\hat{L}_i$. The nonzero elements in $\hat{\boldsymbol{g}}_i$, which is the estimate of $\tilde{\boldsymbol{h}}_i$, can be more specifically expressed by

$$\hat{\tilde{\boldsymbol{h}}}_i = \frac{\hat{\gamma}_i}{\hat{\gamma}_i + \hat{\lambda}} \boldsymbol{v}_{i,\hat{L}_i}. \tag{30}$$

VI. Generalized Likelihood Ratio Test (GLRT)

Since GLRT is widely used for detection problems with unknown parameters, we also discuss GLRT design of D2D neighbor discovery for comparison. The GLRT detector is implemented by replacing the unknown parameters with their ML estimates under each hypothesis. We first discuss the GLRT for Problem (22). To reduce complexity of iterative parameter estimation, we also consider GLRT after the noise variance λ is estimated.

A. GLRT Formulation

For Problem (22), the generalized likelihood ratio is

$$\begin{aligned} L_G(\boldsymbol{p}_i) &= \frac{\max_{\gamma_i,\delta_i,L_i,\lambda} f_{\boldsymbol{p}_i}(\boldsymbol{p}_i \mid \gamma_i, \delta_i, L_i, \lambda)}{\max_{\lambda} f_{\boldsymbol{p}_i}(\boldsymbol{p}_i \mid \gamma_i = 0, \lambda)} \\ &= \frac{\max_{\gamma_i,\delta_i,L_i,\lambda} \frac{\exp\left(-\boldsymbol{p}_i^H \boldsymbol{\Sigma}_{\boldsymbol{p}_i}^{-1} \boldsymbol{p}_i\right)}{\pi^{G+K} \left|\boldsymbol{\Sigma}_{\boldsymbol{p}_i}\right|}}{\max_{\lambda} \frac{\exp\left(-\lambda^{-1} \boldsymbol{p}_i^H \boldsymbol{p}_i\right)}{\pi^{G+K} |\lambda \boldsymbol{I}_{G+K}|}}. \end{aligned}$$

The ML estimate of λ in the denominator (hypothesis $\mathcal{H}_0$) is

$$\hat{\lambda}_0 = \frac{\|\boldsymbol{p}_i\|_2^2}{G+K} = \frac{\|\boldsymbol{v}_i\|_2^2 + \|\boldsymbol{v}_{U+1}\|_2^2}{G+K}.$$

Maximizing the likelihood function in the numerator (hypothesis $\mathcal{H}_1$) is equivalent to minimizing $\xi_S^{(i)} + \xi_S^{(U+1)}$. Since $\hat{L}_i$ and the noise variance under $\mathcal{H}_1$, denoted as $\hat{\lambda}_1$, are dependent, we need to update them iteratively. Starting with

$$\hat{\lambda}_1^{(0)} = \hat{\lambda}_0, \tag{31}$$

if $\max_j v_{ij} \le \hat{\lambda}_0$, then $\hat{L}_i = 0$ and $\hat{\lambda}_1 = \hat{\lambda}_0$. Otherwise, $\hat{L}_i$ can be estimated as

$$\hat{L}_i^{(t)} = \underset{\substack{L_i \in \{1,\ldots,L\} \\ \|\boldsymbol{v}_{i,L_i}\|_2^2 / L_i \ge \hat{\lambda}_1^{(t)}}}{\arg\min} \left\{ L_i \log \frac{\|\boldsymbol{v}_{i,L_i}\|_2^2}{L_i \hat{\lambda}_1^{(t)}} + L_i + \frac{\left\|\boldsymbol{v}_{i,L_i^c}\right\|_2^2}{\hat{\lambda}_1^{(t)}} \right\} \tag{32}$$

and $\hat{\lambda}_1$ is updated by

$$\hat{\lambda}_1^{(t+1)} = \frac{\|\boldsymbol{v}_i\|_2^2 + \|\boldsymbol{v}_{U+1}\|_2^2 - \|\boldsymbol{v}_{i,\hat{L}_i^{(t)}}\|_2^2}{G + K - \hat{L}_i^{(t)}}. \tag{33}$$

Apply (32) and (33) alternatively until convergence. Denote $\hat{L}_i$ and $\hat{\lambda}_1$ as the estimates after convergence, we have

$$\begin{aligned} \log L_G(\boldsymbol{p}_i) = &-(G+K-\hat{L}_i) \log \frac{\left\|\boldsymbol{v}_{i,\hat{L}_i^c}\right\|_2^2 + \|\boldsymbol{v}_{U+1}\|_2^2}{G+K-\hat{L}_i} \\ &+(G+K) \log \frac{\|\boldsymbol{v}_i\|_2^2 + \|\boldsymbol{v}_{U+1}\|_2^2}{G+K} - \hat{L}_i \log \frac{\left\|\boldsymbol{v}_{i,\hat{L}_i}\right\|_2^2}{\hat{L}_i}. \end{aligned}$$

Let $x = \frac{\|\boldsymbol{v}_{i,\hat{L}_i^c}\|_2^2 + \|\boldsymbol{v}_{U+1}\|_2^2}{G+K-\hat{L}_i}$, $y = \frac{\|\boldsymbol{v}_{i,\hat{L}_i}\|_2^2}{\hat{L}_i}$ and $\alpha = \frac{G+K-\hat{L}_i}{G-K}$, $\beta = \frac{\hat{L}_i}{G-K}$. Then $y \ge x$ and $\alpha + \beta = 1$. Further,

$$\begin{aligned} (G+K) L_G(\boldsymbol{p}_i) &= \log(\alpha x + \beta y) - \alpha \log x - \beta \log y \\ &= \log\left(\alpha + \beta \frac{y}{x}\right) - \beta \log \frac{y}{x} \end{aligned}$$

which increases with $\frac{y}{x}$ for $\frac{y}{x} \ge 1$. Therefore we can express the GLRT as

$$(\mathbf{GLRT\ (I)}) \quad \frac{(G+K-\hat{L}_i)\left\|\boldsymbol{v}_{i,\hat{L}_i}\right\|_2^2 / \hat{L}_i}{\left(\left\|\boldsymbol{v}_{i,\hat{L}_i^c}\right\|_2^2 + \|\boldsymbol{v}_{U+1}\|_2^2\right)} \underset{H_0}{\overset{H_1}{\gtrless}} \eta. \tag{34}$$

B. Complexity Reduction

The detection rule (34) depends on $\hat{L}_i$, which can only be obtained iteratively due to the interdependency of $\hat{\lambda}$ and $\hat{L}_i$. For complexity reduction, we can fix the noise level as

$$\hat{\lambda} = \frac{\|\boldsymbol{v}_{U+1}\|_2^2}{K}.$$

Without estimating λ, the generalized likelihood ratio is

$$L_G(\boldsymbol{p}_i) = \frac{\max_{\gamma_i,\delta_i,L_i} f(\boldsymbol{p}_i \mid \gamma_i, \hat{\lambda})}{f(\boldsymbol{p}_i \mid \gamma_i = 0, \hat{\lambda})},$$

where the numerator is maximized by

$$\hat{L}_i = \underset{\substack{L_i \in \{1,\ldots,L\} \\ \|\boldsymbol{v}_{i,L_i}\|_2^2 / L_i \ge \hat{\lambda}}}{\arg\min} \left\{ L_i \log \frac{\|\boldsymbol{v}_{i,L_i}\|_2^2}{L_i \hat{\lambda}} + L_i + \frac{\left\|\boldsymbol{v}_{i,L_i^c}\right\|_2^2}{\hat{\lambda}} \right\},$$

$$\hat{\gamma}_i = \left(\frac{\left\|\boldsymbol{v}_{i,\hat{L}_i}\right\|_2^2}{\hat{L}_i} - \hat{\lambda} \right)^+.$$

As a result,

$$\log L_G(\boldsymbol{p}_i) = \frac{\left\|\boldsymbol{v}_{i,\hat{L}_i}\right\|_2^2}{\hat{\lambda}} - \hat{L}_i \log \frac{\left\|\boldsymbol{v}_{i,\hat{L}_i}\right\|_2^2}{\hat{L}_i \hat{\lambda}} - \hat{L}_i. \tag{35}$$

The GLRT is hence expressed as

$$(\mathbf{GLRT\ (II)}) \quad \log L_G(\boldsymbol{p}_i) \underset{H_0}{\overset{H_1}{\gtrless}} \eta. \tag{36}$$

Note that $\log L_G(\boldsymbol{p}_i)' = 0$ when $\max_j |v_{i,j}|^2 \le \hat{\lambda}$.

C. D2D Channel Estimation

Similar to the discussion in Section V.E, we can use (34) or (36) to obtain the active ZC sequences set $\mathcal{I}$. Then $\hat{\lambda}$ and $\hat{L}_i$ can be updated alternatively starting with (28). Based on the estimated parameters, the channel vectors can be further estimated using (29).

VII. Multi-Antenna Transmission in SRS

In practice, we should also consider how neighbor discovery can be improved when UEs are equipped with multiple antennas. From [12], the cyclic shift of ZC sequence transmitted from the p-th antenna of UE-i is given by

$$\alpha_i^{(p)} = n_i \frac{\left(m_i + \frac{8p}{N_p}\right) \bmod 8}{8}, \quad p = 0, \ldots, N_p - 1. \tag{37}$$

The integer $m_i \in \{0, 1, \ldots, 7\}$ representing multiplexing UEs on the same SRS comb is configured by the higher layer and N_p is the total number of antenna ports used in SRS. Note that when there is only one antenna, i.e., $p = 0$, the cyclic shift is given by $\alpha_i = n_i \frac{m_i}{8}$. Hence, the cyclic shifts of UEs using the same SRS comb are uniformly separated by $\frac{n_i}{8}$. When $N_p \ge 2$, the cyclic shifts of ZC sequences used by different UEs may be the same. However, they will be allocated to RBs on different frequencies, i.e., several SRS combs will be used for each UE with multi-antenna transmission.

A. Maximum Likelihood Estimation

For each SRS comb, the same formulation in Section III can be applied for channel recovery. Assuming that the channel states from different UEs and from different antenna ports of a UE are independent, the objective function of BSBL for the multi-antenna case is

$$\begin{aligned}\xi_S' = \sum_{q=0}^{N_q-1} \sum_{p=0}^{N_p-1} \Bigg\{ \sum_{i=1}^{U} \Bigg[& L_i \log(\lambda + \gamma_i) + \frac{\|\boldsymbol{v}_{q,p,i,L_i}\|_2^2}{\lambda + \gamma_i} \\ & + (G - L_i) \log \lambda + \frac{\left\|\boldsymbol{v}_{q,p,i,L_i^c}\right\|_2^2}{\lambda} \Bigg] \\ & + K \log \lambda + \frac{\|\boldsymbol{v}_{q,p,U+1}\|_2^2}{\lambda} \Bigg\},\end{aligned}$$

where $\boldsymbol{v}_{q,p,i}$ denotes $\boldsymbol{v}_i$ from the p-th transmit antenna to the q-th receive antenna. $\boldsymbol{v}_{q,p,i,L_i}$ is L_i consecutive elements in $\boldsymbol{v}_{q,p,i}$ and $\boldsymbol{v}_{q,p,i,L_i^c}$ is its complement elements. N_q and N_p are the number of receive and transmit antennas, respectively. We assumed that every channel between two UEs has the same statistic $\{\gamma_i, \delta_i, L_i\}$. By changing the order of summation, ξ_S' can be rewritten as

$$\begin{aligned}\xi_S' = {} & N_q N_p \\ & \times \Bigg\{ \sum_{i=1}^{U} \Bigg[L_i \log(\lambda + \gamma_i) + \frac{\|\bar{\boldsymbol{v}}_{i,L_i}\|_2^2}{\lambda + \gamma_i} + (G - L_i) \log \lambda \\ & + \frac{\left\|\bar{\boldsymbol{v}}_{i,L_i^c}\right\|_2^2}{\lambda} \Bigg] + K \log \lambda + \frac{\|\bar{\boldsymbol{v}}_{U+1}\|_2^2}{\lambda} \Bigg\}.\end{aligned} \tag{38}$$

Here we use $\bar{\boldsymbol{v}}_i$ to denote the averaged $\boldsymbol{v}_i$ from all antennas. Each entry of $\bar{\boldsymbol{v}}_i$ is the square root of the averaged squared-amplitude of the corresponding entries in $\boldsymbol{v}_{q,p,i}$. Specifically, let $(\bar{\boldsymbol{v}}_i)_j$ and $(\boldsymbol{v}_{q,p,i})_j$ denote the j-th entry of $\bar{\boldsymbol{v}}_i$ and $\boldsymbol{v}_{q,p,i}$, respectively. Then

$$(\bar{\boldsymbol{v}}_i)_j = \sqrt{\frac{\sum_{q=1}^{N_q} \sum_{p=1}^{N_p} |(\boldsymbol{v}_{q,p,i})_j|^2}{N_q N_p}}, \quad j = 1, \ldots, G.$$

$\bar{\boldsymbol{v}}_{i,L_i}$ denotes the L_i consecutive elements in $\bar{\boldsymbol{v}}_i$ that has the maximum l_2-norm and $\bar{\boldsymbol{v}}_{i,L_i^c}$ is the complement elements of $\bar{\boldsymbol{v}}_{i,L_i}$ in $\bar{\boldsymbol{v}}_i$.

Based on (38), the parameters $\{\{\gamma_i, \delta_i, L_i\}_{i=1}^U, \lambda\}$ can be estimated in a similar manner as in Section V. Compared with the single antenna case, the $\{\|\boldsymbol{v}_{i,L_i}\|^2\}_{i=1}^U$ and $\{\|\boldsymbol{v}_{i,L_i^c}\|^2\}_{i=1}^U$ terms are replaced by $\{\|\bar{\boldsymbol{v}}_{i,L_i}\|^2\}_{i=1}^U$ and $\{\|\bar{\boldsymbol{v}}_{i,L_i^c}\|^2\}_{i=1}^U$. Consequently,

$$\hat{L}_i = \underset{\substack{L_i \in \{1,\ldots,L\} \\ \|\bar{\boldsymbol{v}}_{i,L_i}\|_2^2 / L_i \ge \lambda}}{\arg\min} \left\{ L_i \log \frac{\|\bar{\boldsymbol{v}}_{i,L_i}\|_2^2}{L_i \lambda} + L_i + \frac{\left\|\bar{\boldsymbol{v}}_{i,L_i^c}\right\|_2^2}{\lambda} \right\}. \tag{39}$$

$$\hat{\lambda} = \frac{\sum_{i=1}^{U} \|\bar{\boldsymbol{v}}_i\|_2^2 + \|\bar{\boldsymbol{v}}_{U+1}\|_2^2 - \sum_{i \in \mathcal{I}} \|\bar{\boldsymbol{v}}_{i,\hat{L}_i}\|_2^2}{UG + K - \sum_{i \in \mathcal{I}} \hat{L}_i}. \tag{40}$$

The position of $\bar{\boldsymbol{v}}_{i,\hat{L}_i}$ in $\bar{\boldsymbol{v}}_i$ characterizes $\hat{\delta}_i$. Using (39) and (40), $\hat{\lambda}$ and $\{\hat{L}_i\}_{i=1}^U$ can be updated iteratively. Let $\boldsymbol{g}_{q,p,i}$ denote $\boldsymbol{g}_i$ from the p-th antenna of UE-i to the q-th antenna of UE-0. Then it is estimated as

$$\hat{\boldsymbol{g}}_{q,p,i} = \hat{\Sigma}_{\boldsymbol{g}_{q,p,i}} \left(\hat{\Sigma}_{\boldsymbol{g}_{q,p,i}} + \hat{\lambda} \boldsymbol{I}_G \right)^{-1} \boldsymbol{v}_{q,p,i}.$$

Since $\hat{\gamma}_i$ and $\hat{\delta}_i$ are the same for every channel from UE-i, $\hat{\Sigma}_{\boldsymbol{g}_{q,p,i}}$ are equal for different q and p.

B. Composite Hypothesis Testing

Based on the same system model discussed in Section VII.A, the binary hypothesis testing rules for the multi-antenna case can be modified from the single antenna case by replacing the $\boldsymbol{v}_i$ terms with their $\bar{\boldsymbol{v}}_i$ counterparts. We summarized the detection rules in Table II. For comparison, the idealized Neyman-Pearson (NP) test where all parameters are assumed to be known as well as the UMPI tests with partially known statistics are also listed. After characterizing $\mathcal{I}$ using the binary hypothesis testing

TABLE II
DETECTION RULES

	Single Antenna	**Multiple Antennas**
NP test	$\frac{\|\boldsymbol{v}_{i,L_i}\|_2^2}{L_i} \underset{H_0}{\overset{H_1}{\gtrless}} \eta$	$\frac{\|\overline{\boldsymbol{v}}_{i,L_i}\|_2^2}{L_i} \underset{H_0}{\overset{H_1}{\gtrless}} \eta$
UMPI (I) (known δ_i, L_i)	$\frac{\|\boldsymbol{v}_{i,L_i}\|_2^2}{\|\boldsymbol{v}_i\|_2^2+0.5\|\boldsymbol{v}_{U+1}\|_2^2} \underset{H_0}{\overset{H_1}{\gtrless}} \eta$	$\frac{\|\overline{\boldsymbol{v}}_{i,L_i}\|_2^2}{\|\overline{\boldsymbol{v}}_{i,L_i}\|_2^2+0.5\|\overline{\boldsymbol{v}}_{U+1}\|_2^2} \underset{H_0}{\overset{H_1}{\gtrless}} \eta$
UMPI (II) (known SNR, L_i)	$\sum_{j=1}^{G}\left[1-\frac{\left(1-\frac{1}{\gamma_i/\lambda+1}\right)\|(\boldsymbol{v}_i)_{j,L_i}\|_2^2}{\|\boldsymbol{v}_i\|_2^2+0.5\|\boldsymbol{v}_{U+1}\|_2^2}\right]^{-(K+0.5)} \underset{H_0}{\overset{H_1}{\gtrless}} \eta$	$\sum_{j=1}^{G}\left[1-\frac{\left(1-\frac{1}{\gamma_i/\lambda+1}\right)\|(\overline{\boldsymbol{v}}_i)_{j,L_i}\|_2^2}{\|\overline{\boldsymbol{v}}_i\|_2^2+0.5\|\overline{\boldsymbol{v}}_{U+1}\|_2^2}\right]^{-(K+0.5)} \underset{H_0}{\overset{H_1}{\gtrless}} \eta$
LMPI	$\frac{\|\boldsymbol{v}_i\|_2^2/G}{\|\boldsymbol{v}_{U+1}\|_2^2/K} \underset{H_0}{\overset{H_1}{\gtrless}} \eta$	$\frac{\|\overline{\boldsymbol{v}}_i\|_2^2/G}{\|\overline{\boldsymbol{v}}_{U+1}\|_2^2/K} \underset{H_0}{\overset{H_1}{\gtrless}} \eta$
CFAR	$\sum_{j=1}^{G}\left(1-\frac{\|v_{i,j}\|_2^2}{\|\boldsymbol{v}_i\|_2^2+0.5\|\boldsymbol{v}_{U+1}\|_2^2}\right)^{-(K+0.5)} \underset{H_0}{\overset{H_1}{\gtrless}} \eta$	$\sum_{j=1}^{G}\left(1-\frac{\|\overline{v}_{i,j}\|_2^2}{\|\overline{\boldsymbol{v}}_i\|_2^2+0.5\|\overline{\boldsymbol{v}}_{U+1}\|_2^2}\right)^{-(K+0.5)} \underset{H_0}{\overset{H_1}{\gtrless}} \eta$
GLRT (I)	$\frac{(G-\hat{L}_i+K)\|\boldsymbol{v}_{i,\hat{L}_i}\|_2^2/\hat{L}_i}{\|\boldsymbol{v}_{i,\hat{L}_i^c}\|_2^2+\|\boldsymbol{v}_{U+1}\|_2^2} \underset{H_0}{\overset{H_1}{\gtrless}} \eta$	$\frac{(G-\hat{L}_i+K)\|\overline{\boldsymbol{v}}_{i,\hat{L}_i}\|_2^2/\hat{L}_i}{\|\overline{\boldsymbol{v}}_{i,\hat{L}_i^c}\|_2^2+\|\overline{\boldsymbol{v}}_{U+1}\|_2^2} \underset{H_0}{\overset{H_1}{\gtrless}} \eta$
GLRT (II)	$\frac{\|\boldsymbol{v}_{i,\hat{L}_i}\|_2^2}{\hat{\lambda}} - \hat{L}_i \log\frac{\|\boldsymbol{v}_{i,\hat{L}_i}\|_2^2}{\hat{L}_i\hat{\lambda}} - \hat{L}_i \underset{H_0}{\overset{H_1}{\gtrless}} \eta$	$\frac{\|\overline{\boldsymbol{v}}_{i,\hat{L}_i}\|_2^2}{\hat{\lambda}} - \hat{L}_i \log\frac{\|\overline{\boldsymbol{v}}_{i,\hat{L}_i}\|_2^2}{\hat{L}_i\hat{\lambda}} - \hat{L}_i \underset{H_0}{\overset{H_1}{\gtrless}} \eta$

rules, λ and $\{\gamma_i, \delta_i, L_i, \boldsymbol{g}_i\}_{i=1}^{U}$ can be estimated following similar discussion in Section V.E.

VIII. NUMERICAL RESULTS

In this section, we will provide numerical results to evaluate the performance of neighbor discovery methods. We first depict the receive operating characteristic (ROC) curves of the discussed detection methods as a benchmark for comparing the detection performance. Then we describe the LTE system and parameters used for practical neighbor discovery simulation. The methods we propose are then evaluated with regards to various network parameters.

A. Receiver Operating Characteristic

In Fig. 3, we show the ROC curves of invariant tests and GLRT (I), which are compared with NP test and UMPI tests given in Table II. The NP test is derived under the circumstance where all the parameters in $\boldsymbol{\theta}$ are known. It is optimal in the sense that it gives the highest detection probability among all tests for a fixed false alarm rate. The two UMPI tests in Table II are derived by assuming certain parameters in $\boldsymbol{\theta}$ are known.

More information about the parameters contributes to better detection performance, hence the NP test has the best performance. For UMPI tests, the result in Fig. 3 shows that information about δ_i, i.e., propagation delay, is more critical in improving detection accuracy. While the CFAR test has nearly the same ROC curve with UMPI (II), the LMPI test does not perform as well. The ROC curve of GLRT (I) is also below CFAR.

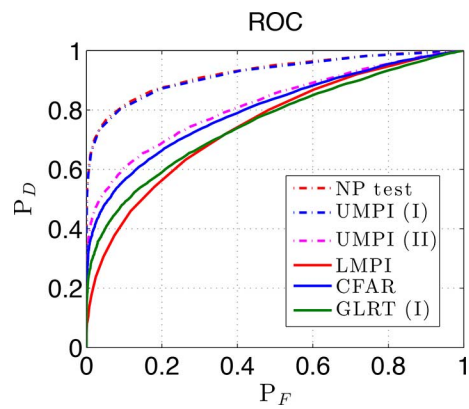

Fig. 3. Receiver operating characteristic (ROC) curves of neighbor discovery methods in SRS. $10\log(\gamma_i/\lambda) = 6$ dB.

B. LTE Parameters

The channel parameters following LTE standards [11], [12] are provided in Table III. For the simulation results presented in the paper, we considered two SRS combs and hence in total 16 possible SRS transmitters. Due to IFDMA, each SRS comb is composed of 576 subcarriers, which is half of the SRS bandwidth. In Table IV, $\boldsymbol{x}_i$ denotes the parameters in (2), which is based on 2048-point DFT assumed for uplink SC-FDMA. $\boldsymbol{s}_i$ denotes the corresponding size parameters in (4) for a SRS comb. L_{CP}, L_x and $\delta_{\max,x}$ are calculated based on the CP duration, maximum delay spread and maximum round trip delay in Table III.

In LTE, the transmission power of each UE is adjusted such that each uplink maintains a fixed SNR at the eNB. From the path loss model in Table III, UEs located further from the eNB will adopt higher transmission power. Denote the target uplink SNR as $\mathrm{SNR}_T[dB]$. The transmission power $[dB]$ of UE-i with uplink path loss PL_i is calculated as

$$P_{T,i}[dB] = \mathrm{SNR}_T[dB] + \mathrm{PL}_i[dB] + \sigma_n^2[dB].$$

PL_i and the noise variance σ_n^2 are listed in Table III. We consider neighbor discovery process within one cell where 10 out

TABLE III
SIMULATION PARAMETERS

D2D path loss	148 + 40*log10(d[km])
uplink path loss	128.1 + 37.6*log10(d[km])
noise variance [dB]	-174+10*log10(BW)+NF-30
noise figure (NF)	7
bandwidth (BW)	20MHz (100 RB)
DFT size	2048
SRS bandwidth	96 RB (1152 subcarriers)
ZC sequence length	571
Cyclic prefix duration	160 Ts (5.2us)
maximum delay spread	0.5 us (ETU model)
cell radius	600 m
maximum round trip delay	4 us

TABLE IV
SIZE PARAMETERS

$\boldsymbol{x}_i$	$N = 2048$	$L_{\mathrm{CP}} = 160$	$L_x = 16$	$\delta_{\max,x} = 124$
$\boldsymbol{s}_i$	$n_i = 571$	$G = 40$	$L = 5$	$\delta_{\max} = 35$
	cyclic shift = 71		$U = 16$	$K = 502$

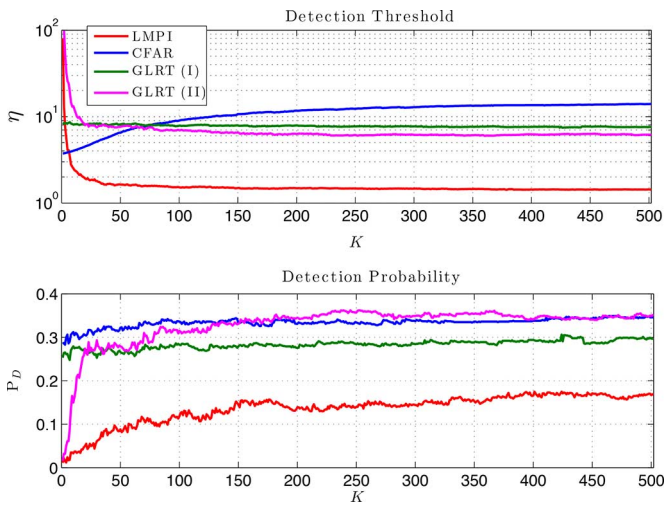

Fig. 4. Detection threshold and detection probability for $\mathrm{P}_F = 0.01$. $10\log(\gamma_i/\lambda) = 6$ dB.

of 16 possible SRS transmitters are actively transmitting. The locations of the transmitters are uniformly generated over an area of 600 m × 600 m square centered at the eNB. UE-0 is assumed 300 m away from the eNB. One possible realization of the network deployment is depicted in Fig. 5. The channel vectors and the noise vector are generated randomly following the complex Gaussian model given in Section III. Each simulation consists of 1000 trials.

C. Neighbor Discovery Performance

Next we will present the numeral results of the neighbor discovery methods proposed in the paper for the LTE system setup discussed above.

1) Dimension of the Noise Subspace: In Fig. 4, we evaluate the impact of the dimension of the noise subspace (K) on the detection probability. The detection thresholds in the upper subfigure are set by fixing $\mathrm{P}_F = 0.01$ among 1000 independent channel realizations. The corresponding detection probability with channel variance satisfying $10\log(\gamma_i/\lambda) = 6$ dB is depicted in the lower subfigure. Overall, larger K will lead to better detection performance. The value of K has more impact

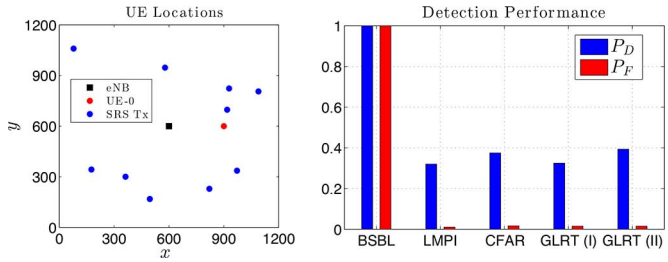

Fig. 5. Network deployment and the corresponding detection performance of various neighbor discovery methods. $\mathrm{SNR}_T = 20$ dB.

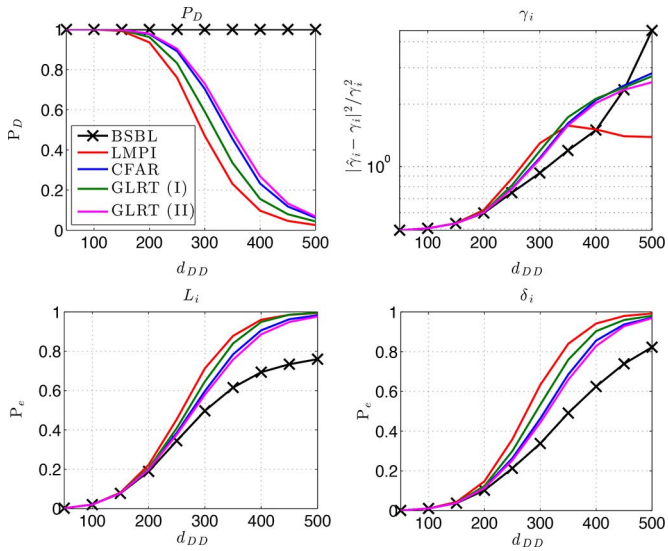

Fig. 6. Detection and parameter estimation performance varying with the distance between the transmitter and UE-0. The thresholds for LMPI, CFAR and the two GLRT methods are set with $P_F = 0.01$.

on the performance of GLRT (II) since this method estimates the noise variance directly from the noise subspace.

2) Active ZC Sequence Detection: In Fig. 5, we implemented different neighbor detection methods for the network depicted in the left subfigure. The locations of the 10 SRS transmitters (SRS Txs) are randomly generated from uniform distribution. The subfigure on the right-hand side (RHS) plots the detection and false alarm probability of different methods. We chose thresholds for the detection rules of the last four methods by setting $P_F = 0.01$.

Among 1000 trials, we found that BSBL always detects all 16 possible SRS transmitters, which results in $P_D = P_F = 1$. From (17), UE-i is detected in BSBL whenever $\max_j |v_{i,j}|^2 \geq \lambda$. As λ estimated in (18) is the averaged squared-amplitude of the noise taps, $\max_j |v_{i,j}|^2 \geq \frac{\|\boldsymbol{v}_i\|_2^2}{G} \approx \lambda$ for all i. Therefore, BSBL cannot distinguish active ZC sequences from inactive ones. On the contrary, for the other four detection methods, the false alarm rate can be reduced by setting higher detection thresholds.

3) Transmitter Location: In Fig. 6, we considered one SRS transmitter with fixed transmission power while its distance from UE-0, denoted as d_{DD}, varies from 50 m to 500 m. The MSE of γ_i is calculated as $|\hat{\gamma}_i - \gamma_i|^2/\gamma_i^2$. The two subfigures in the second row evaluate the estimation error probability of L_i and δ_i. From the figure, both the detection and estimation

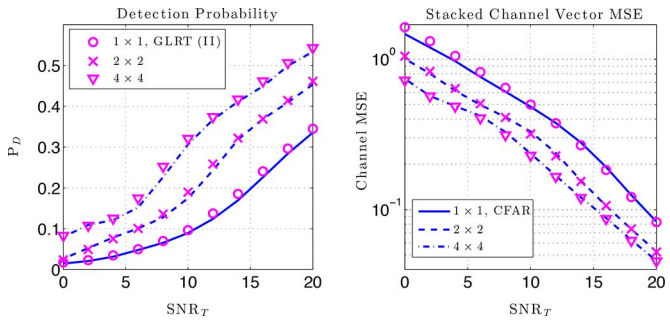

Fig. 7. The neighbor discovery performance as a function of the transmission power of scheduled transmitters in SRS.

performance deteriorates with the increasing of d_{DD}. In the second subfigure, the MSE of γ_i for LMPI drops in the range $300\text{ m} \leq d_{DD} \leq 500\text{ m}$ due to its low detection probability. $|\hat{\gamma}_i - \gamma_i|^2/\gamma_i^2 = 1$ when $\hat{\gamma}_i = 0$. While for other methods, nonzero $\hat{\gamma}_i$ leads to large MSE due to small γ_i.

4) Transmission Power: We plot the active ZC sequence detection probability and stacked channel vector MSE as a function of SNR_T in Fig. 7. The network deployment follows from Fig. 5. The channel MSE in the RHS subfigure is calculated by $\|\boldsymbol{g} - \hat{\boldsymbol{g}}\|_2^2/(\sum_{i=1}^{U} L_i\gamma_i)$, which captures both detection error and estimation error of all the parameters. $N_q \times N_p$ denote the number of receive and transmit antennas. Naturally, higher transmission power lead to better performance of the system. Moreover, as seen from the figure, multiple antennas can improve both detection and sparse channel recovery accuracy.

IX. Conclusion

In this paper, we studied the problem of neighbor discovery for enabling direct UE communication in standard LTE cellular networks. Our work demonstrates that users in the cellular network can detect their neighbors by simply listening to their uplink transmissions. We compare different uplink channels in the LTE system and propose SRS and PRACH as potential neighbor discovery opportunities due to their common LTE structure to all the users.

Our work focuses on statistical methods for simultaneous neighbor detection and D2D channel estimation. Due to the fact that the channel parameters are unknown to the discovering UE, we propose several methods for neighbor discovery in SRS using the framework of block sparse bayesian learning and composite hypothesis testing in detection theory. The estimated D2D channel during neighbor discovery process can be utilized for later D2D communications. We evaluate the neighbor discovery performance with regards to various system parameters in practical LTE deployment.

For future works, we consider neighbor discovery in PRACH. Since different-root ZC sequences are used as preambles in PRACH, the orthogonality of $\boldsymbol{\Psi}$ cannot be preserved. Therefore, we need different methods for enabling neighbor discovery in PRACH. Moreover, besides the statistical approach, the problem can also be examined from a compressive sensing viewpoint by recovering a deterministic sparse vector.

Appendix A
Proof of Theorem 1

We start with proving $S(g(\boldsymbol{p}_i)) = S(\boldsymbol{p}_i)$. Substituting $g(\boldsymbol{p}_i) = c\boldsymbol{A}\boldsymbol{p}_i$ into the expression of $S(\boldsymbol{p}_i)$ in (24), we have

$$S(g(\boldsymbol{p}_i)) = \frac{\boldsymbol{P}_{j_*'} c\boldsymbol{P}_j \boldsymbol{v}_i}{\|c\boldsymbol{A}_2\boldsymbol{v}_{U+1}\|_2} = \frac{\boldsymbol{P}_{j_*'}\boldsymbol{P}_j\boldsymbol{v}_i}{\|\boldsymbol{v}_{U+1}\|_2}.$$

Note that $\boldsymbol{P}_j\boldsymbol{v}_i$ is a cyclic shifted version of $\boldsymbol{v}_i$. After applying $\boldsymbol{P}_{j_*'}$, the first L elements of $\boldsymbol{v}_i$ has the maximum l_2-norm among all L circularly consecutive elements of $\boldsymbol{v}_i$. Hence, $\boldsymbol{P}_{j_*'}\boldsymbol{P}_j\boldsymbol{v}_i = \boldsymbol{P}_{j_*}\boldsymbol{v}_i$. As a result, $S(g(\boldsymbol{p}_i)) = \frac{\boldsymbol{P}_{j_*}\boldsymbol{v}_i}{\|\boldsymbol{v}_{U+1}\|_2} = S(\boldsymbol{p}_i)$.

To claim that $S(\boldsymbol{p}_i)$ is a maximal statistic, it is also necessary to show that $S(\boldsymbol{p}_i') = S(\boldsymbol{p}_i)$ implies $\boldsymbol{p}_i' = g(\boldsymbol{p}_i)$ for some $g \in \mathcal{G}$. From $S(\boldsymbol{p}_i') = S(\boldsymbol{p}_i)$, it holds that

$$\frac{\boldsymbol{P}_{j_*}\boldsymbol{v}_i}{\|\boldsymbol{v}_{U+1}\|_2} = \frac{\boldsymbol{P}_{j_*'}\boldsymbol{v}_i'}{\|\boldsymbol{v}_{U+1}'\|_2}.$$

Equivalently,

$$\boldsymbol{P}_{j_*'}\boldsymbol{v}_i' = \frac{\|\boldsymbol{v}_{U+1}'\|_2}{\|\boldsymbol{v}_{U+1}\|_2} \cdot \boldsymbol{P}_{j_*}\boldsymbol{v}_i =: c\boldsymbol{P}_{j_*}\boldsymbol{v}_i.$$

Therefore,

$$\boldsymbol{v}_i' = c\boldsymbol{P}_{j_*'}^T\boldsymbol{P}_{j_*}\boldsymbol{v}_i, \tag{41}$$

i.e., $\boldsymbol{v}_i'$ is cyclically shifted from $\boldsymbol{v}_i$. Moreover, since

$$\frac{\|\boldsymbol{v}_{U+1}'\|_2}{\|\boldsymbol{v}_{U+1}\|_2} = c, \tag{42}$$

it implies that

$$\boldsymbol{v}_{U+1}' = c\boldsymbol{A}_2\boldsymbol{v}_{U+1} \tag{43}$$

for some unitary matrix $\boldsymbol{A}_2$. More specifically, from [17], denote the singular value decomposition (SVD) of $\boldsymbol{v}_{U+1}$ and $\boldsymbol{v}_{U+1}'$ by

$$\boldsymbol{v}_{U+1} = \underbrace{\left[\boldsymbol{v}_{U+1}/\|\boldsymbol{v}_{U+1}\|_2 \quad \boldsymbol{U}_{U+1}^{\dagger}\right]}_{\boldsymbol{U}_{U+1}} \underbrace{\begin{bmatrix}\|\boldsymbol{v}_{U+1}\|_2 \\ \boldsymbol{0}\end{bmatrix}}_{\boldsymbol{d}_{U+1}}$$

$$\boldsymbol{v}_{U+1}' = \underbrace{\left[\boldsymbol{v}_{U+1}'/\|\boldsymbol{v}_{U+1}'\|_2 \quad \boldsymbol{U}_{U+1}^{'\dagger}\right]}_{\boldsymbol{U}_{U+1}'} \underbrace{\begin{bmatrix}\|\boldsymbol{v}_{U+1}'\|_2 \\ \boldsymbol{0}\end{bmatrix}}_{\boldsymbol{d}_{U+1}'}$$

then $\boldsymbol{A}_2$ can be taken as $\boldsymbol{A}_2 = \boldsymbol{U}_{U+1}'\boldsymbol{U}_{U+1}^H$. $\boldsymbol{A}_2$ is unitary since $\boldsymbol{A}_1^H\boldsymbol{A}_1 = \boldsymbol{U}_{U+1}(\boldsymbol{U}_{U+1}')^H\boldsymbol{U}_{U+1}'\boldsymbol{U}_{U+1}^H = \boldsymbol{I}_K$. Moreover,

$$c\boldsymbol{A}_2\boldsymbol{v}_{U+1} = c\boldsymbol{U}_{U+1}'\boldsymbol{U}_{U+1}^H\boldsymbol{v}_{U+1} = c\boldsymbol{U}_{U+1}'\begin{bmatrix}\|\boldsymbol{v}_{U+1}\|_2 \\ \boldsymbol{0}\end{bmatrix} = \boldsymbol{v}_{U+1}'.$$

Hence, there exists a unitary transformation between $\boldsymbol{v}_{U+1}$ and $\boldsymbol{v}_{U+1}'$ given the relationship in (42). From (41) and (43), it holds that $\boldsymbol{p}_i' = c\boldsymbol{A}\boldsymbol{p}_i$ for some $\boldsymbol{A} \in \mathcal{A}$. Hence, $S(\boldsymbol{p}_i)$ is a maximal invariant statistic.

REFERENCES

[1] 3GPP, "3rd generation partnership project; technical specification group SA; feasibility study for proximity services(ProSe) (Release 12)," Tech. Rep. 22.803 V1.0.0, Aug. 2012.

[2] L. Lei, Z. Zhong, C. Lin, and X. Shen, "Operator controlled device-to-device communications in LTE-advanced networks," *IEEE Wireless Commun.*, vol. 19, no. 3, pp. 96–104, Jun. 2012.

[3] K. Doppler, C. B. Ribeiro, and J. Kneckt, "Advances in D2D communications: Energy efficient service and device discovery radio," in *Proc. IEEE Wireless VITAE*, Mar. 2011, pp. 1–6.

[4] Intel, "Discussion on design options for D2D discovery," Tech. Rep. R1-131924, May 2013.

[5] B. Kaufman, B. Aazhang, and J. Lilleberg, "Interference aware link discovery for device to device communication," presented at the Asilomar Conf. Signals, Syst., Comput., Nov. 2009.

[6] F. Baccelli, N. Khude, R. Laroia, J. Li, T. Richardson, S. Shakkottai, S. Tavildar, and X. Wu, "On the design of device-to-device autonomous discovery," in *Proc. Int. Conf. Commun. Syst. Netw.*, Jan. 2012, pp. 1–9.

[7] D. Angelosante, E. Biglieri, and M. Lops, "Neighbor discovery in wireless networks: A multiuser-detection approach," *Phys. Commun.*, vol. 3, no. 1, pp. 28–36, Mar. 2010.

[8] H. Zhu and G. B. Giannakis, "Exploiting sparse user activity in multiuser detection," *IEEE Trans. Commun.*, vol. 59, no. 2, pp. 454–465, Feb. 2011.

[9] C. Bockelmann, H. F. Schepker, and A. Dekorsy, "Compressive sensing based multi-user detection for machine-to-machine communication," *Trans. Emerg. Telecommun. Technol.*, vol. 24, no. 4, pp. 389–400, Jun. 2013.

[10] A. K. Fletcher, S. Rangan, and V. K. Goyal, "On-Off Random Access Channels: A Compressed Sensing Framework," Mar. 2009 [Online]. Available: http://arxiv.org/abs/0903.1022

[11] S. Sesia, I. Toufik, and M. Baker, *LTE: The UMTS Long Term Evolution*. New York, NY, USA: Wiley, 2009.

[12] 3GPP, "Evolved Universal Terrestrial Radio Access (E-UTRA); Physical channels and modulation (Release 11)," 3GPP TSG RAN TS 36.211, v 11.3.0, Jul. 2013.

[13] Z. Zhang and B. Rao, "Sparse signal recovery with temporally correlated source vectors using sparse Bayesian learning," *IEEE J. Sel. Topics Signal Process*, vol. 5, no. 5, pp. 912–926, Sep. 2011.

[14] Z. Zhang and B. Rao, "Extension of SBL algorithms for the recovery of block sparse signals with intra-block correlation," *IEEE Trans. Signal Process.*, vol. 61, no. 8, pp. 2009–2015, Aug.. 2013.

[15] L. Applebaum, W. U. Bajwa, M. F. Duarte, and R. Calderbank, "Multiuser detection in asynchronous on-off random access channels using lasso," *Phys. Commun.*, vol. 5, no. 2, pp. 129–147, June 2012.

[16] B. C. Levy, *Principles of Signal Detection and Parameter Estimation*. Berlin, Germany: Springer-Verlag, 2008.

[17] S. Kraut, L. L. Scharf, and R. W. Butler, "The adaptive coherence estimator: A uniformly most-powerful-invariant adaptive detection statistic," *IEEE Trans. Signal Process.*, vol. 53, no. 2, pp. 427–438, Feb. 2005.

[18] F. Nicolls and G. De Jager, "Uniformly most powerful cyclic permutation invariant detection for discrete-time signals," in *Proc. IEEE Int. Conf. Acoust., Speech, Signal Process.*, May 2001, vol. 5, pp. 3165–3168.

[19] D. Ramírez, J. Vía, I. Santamaría, and L. L. Scharf, "Locally most powerful invariant tests for correlation and sphericity of Gaussian vectors," *IEEE Trans. Inf. Theory*, vol. 59, no. 4, pp. 2128–2141, Apr. 2013.

[20] P. Bertrand, "Channel gain estimation from sounding reference signal in LTE," presented at the IEEE 73rd Veh. Technol. Conf. (VTC Spring), May 2011.

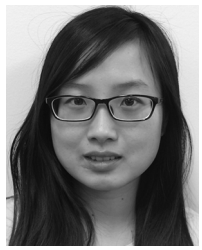

Huan Tang (S'13) received the B.S. degree from Shanghai Jiaotong University, China in 2011. She is currently working towards the Ph.D. degree in the Department of Electrical and Computer Engineering of University of California, Davis.

Her research interests are in the broad area of wireless communication and signal processing with current focus on transceiver design, neighbor discovery and resource allocation of device-to-device communication.

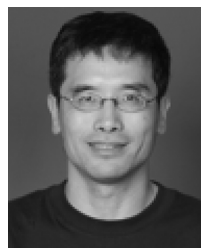

Zhi Ding (S'88–M'90–SM'95–F'03) is Professor of Engineering and Entrepreneurship at the University of California, Davis. He received his Ph.D. degree in electrical engineering from Cornell University in 1990. From 1990 to 2000, he was a faculty member of Auburn University and later, University of Iowa. Prof. Ding has held visiting positions in Australian National University, Hong Kong University of Science and Technology, NASA Lewis Research Center and USAF Wright Laboratory. Prof. Ding has active collaboration with researchers from several countries including Australia, China, Japan, Canada, Taiwan, Korea, Singapore, and Hong Kong.

Dr. Ding is a Fellow of IEEE and has been an active member of IEEE, serving on technical programs of several workshops and conferences. He was associate editor for IEEE TRANSACTIONS ON SIGNAL PROCESSING from 1994–1997, 2001–2004, and associate editor of IEEE SIGNAL PROCESSING LETTERS 2002–2005. He was a member of technical committee on Statistical Signal and Array Processing and member of technical committee on Signal Processing for Communications (1994–2003). Dr. Ding was the Technical Program Chair of the 2006 IEEE Globecom. He is also an IEEE Distinguished Lecturer (Circuits and Systems Society, 2004–06, Communications Society, 2008–09). He served on as IEEE TRANSACTIONS ON WIRELESS COMMUNICATIONS Steering Committee Member (2007–2009) and its Chair (2009–2010). Dr. Ding received the 2012 IEEE Wireless Communication Recognition Award from the IEEE Communications Society and is a coauthor of the text: *Modern Digital and Analog Communication Systems*, 4th edition, Oxford University Press, 2009.

Bernard C. Levy (S'74–M'78–SM'90–F'94) received the diploma of Ingénieur Civil des Mines from the Ecole Nationale Supérieure des Mines in Paris, France in 1974, and the Ph.D. in electrical engineering from Stanford University in 1979.

From July 1979 to June 1987 he was Assistant and then Associate Professor in the Department of Electrical Engineering and Computer Science at M.I.T. Since July 1987, he has been with the University of California at Davis, where he is Professor of Electrical Engineering and a member of the Graduate Group in Applied Mathematics. He served as Chair of the Department of Electrical and Computer Engineering at UC Davis from 1996 to 2000. He was a Visiting Scientist at the Institut de Recherche en Informatique et Systèmes Aléatoires (IRISA) in Rennes, France from January to July 1993, and at the Institut National de Recherche en Informatique et Automatique (INRIA), in Rocquencourt, France, from September to December 2001. He is the author of the book *Principles of Signal Detection and Parameter Estimation* (New York, NY: Springer, 2008). His research interests include statistical signal processing, estimation, detection, and circuits applications of signal processing.

Dr. Levy served as Associate Editor of the IEEE TRANSACTIONS ON CIRCUITS AND SYSTEMS I, of the IEEE TRANSACTIONS ON CIRCUITS AND SYSTEMS II, and of the *EURASIP Journal on Advances in Signal Processing*. He is currently an Associate Editor of Signal Processing. He is a member of SIAM.